MITSUBISHI ELECTRIC RESEARCH LABORATORIES
http://www.merl.com

Performance Analysis of Finite-Sized Cooperative Systems with Unreliable Backhaul Links

Kim, K.J.; Orlik, P.V.; Khan, T.

TR2016-094 July 2016

Abstract

This paper presents a performance analysis of a finite-sized co-operative wireless system, where a group of transmitters with unreliable backhauls serve a desired receiver using noncoherent joint transmission. To facilitate analysis, an analytical expression for the distribution of the spatially averaged signal-to-interference-plus-noise ratio (SA-SINR) is derived in terms of key system and channel parameters. Leveraging the derived expression, the joint impact of node co-operation, backhaul reliability, interference, and communication range is investigated in the considered finite-sized co-operative system. Furthermore, based on the SA-SINR, closed form expressions for the average bit error rate (ABER) and average spectral efficiency (ASE) are derived. Further insights are established by analyzing the asymptotic performance in the high transmission power regime. From analytical derivations for the outage probability, ABER, and ASE and link-level simulations, it is verified that these asymptotic performance metrics are exclusively influenced by unreliable backhauls, so that the conventional diversity gains are not achievable.

IEEE Transactions on Wireless Communications

Performance Analysis of Finite-Sized Cooperative Systems with Unreliable Backhaul Links

Kyeong Jin Kim, *Senior Member, IEEE,*, Philip V. Orlik, *Senior Member, IEEE,* and Talha Ahmed Khan, *Student Member, IEEE*

***Abstract*—This paper presents a performance analysis of a finite-sized cooperative wireless system, where a group of transmitters with unreliable backhaul links serve a desired receiver using non-coherent joint transmission. To facilitate analysis, an analytical expression for the distribution of the spatially averaged signal-to-interference-plus-noise ratio (SA-SINR) is derived in terms of key system and channel parameters. Leveraging the derived expression, the joint impact of node cooperation, backhaul reliability, interference and communication range is investigated in the considered finite-sized cooperative system. Furthermore, based on the SA-SINR, closed form expressions for the average bit error rate (ABER) and average spectral efficiency (ASE) are derived. Further insights are established by analyzing the asymptotic performance in the high transmission power regime. From analytical derivations for the outage probability, ABER, and ASE and link-level simulations, it is verified that these asymptotic performance metrics are exclusively influenced by unreliable backhauls, so that the conventional diversity gains are not achievable.**

***Index Terms*—Wireless backhaul link, backhaul reliability, aggregate interference, safety zone, outage probability, average bit error rate, average spectral efficiency, convergence rate, Nakagami-m fading.**

I. Introduction

BACKHAUL can be referred to as the data transporting process in either direction between the control unit (CU) and a cluster of transmitters to provide broadband communications to the core network [1], [2]. The backhaul link is typically recognized as a high reliable link meeting the requisite quality of service requirement of the terminals [1], [2]. To achieve a higher data rate, extreme densification by mixing a few large cells and many small cells is required [3]. Due to heterogeneous demand from small cells, deployment of cost effective, reliable, and scalable backhaul becomes a challenging problem [3]. Especially, conventional wired backhaul deployment is not cost effective in the emerging wireless network paradigm due to excessive capital investment. As an alternative, wireless backhaul comes across as a cost effective solution. However, due to increased likelihood of non-line-of-sight (nLOS) connections and fading [4], wireless backhaul is unlikely to be as reliable as the wired backhaul [5].

Taking into account limited network resources such as bandwidth and capacity, several works have investigated the effects of wireless backhaul on the system performance. For a non-cellular network, where distributed relay nodes are connected to the destination via finite-rate but unreliable backhaul links, the authors in [6] establish the rate-distortion region in the context of source reconstruction and the authors in [7] investigate the average achievable rate of data transmission over a cooperative relaying network. Also, for a finite backhaul capacity, limited uplink cooperation based on data sharing is proposed in [8]. For two source nodes connected by orthogonal limited-rate error free backhauls, the outer bound on the capacity region for the multicast relay work is derived in [9]. Furthermore, in [10], the authors investigate cooperative network coding for relay-assisted two sources and two destinations networks with an ideal backhaul connection between the source nodes. Several schemes such as distributed compression [11], distributed decoding by exchanging decoded data bits [12], and decentralized decoding [13] are proposed for uplink joint processing. For a coordinated multi-point system, the downlink with unreliable backhaul is considered in [14]. These works have shown that unreliable backhaul severely affects the performance gain promised by cooperative communications.

Today, almost every smart device and vehicular communication equipment contain a global positioning system (GPS) receiver which is capable of determining the radios position to an accuracy of a few centimeters. Additionally, the position information is continuously tracked by cellular service providers and can also be shared with other users in the network. Since now it is easy to gather position information for the terminals within a network, the proposed system model utilizes position information in controlling the interfering terminals. To protect the receiver from serious interference caused by multiple interferers nearby the receiver, a safety zone is formed around the receiver, which is also proposed in the cognitive radio network literature [15]–[17] to protect the primary user. Inside this safety zone, interferes are not allowed to transmit to other nodes. By maintaining a desired ergodic signal-to-interference-plus-noise ratio (SINR) at the receiver, a higher capacity can be achieved [18]. Comparing with existing works, our main contributions are summarized as follows.

Contributions:

- There is a need to accurately evaluate the overall performance of a finite-sized cooperative system in terms of key design parameters such as the number of transmitters,

Manuscript received April 30, 2015; revised August 17, 2015 and February 2, 2016; accepted March 23, 2016. The editor coordinating the review of this paper and approving it for publication was Prof. T. Lok.

K. J. Kim and P. V. Orlik are with Mitsubishi Electric Research Laboratories (MERL), Cambridge, MA, USA.

T. A. Khan is with University of Texas at Austin, TX. The work of T. A. Khan was done while he was an intern in MERL.

number of interferers, and safety zone size over the communication range. Thus, motivated by the works in [15], [19], [20], [21], and [22], we provide an analytical framework to aid the performance evaluation/design of a finite-sized cooperative system, while accounting for the backhaul reliability[1] and interference. The employed channel model is fairly general since this allows for Nakagami-m fading links that may have different fading parameters. For these key heterogeneous parameters, the closed expression for the outage probability is derived.

- The average bit error rate (ABER) and average spectral efficiency (ASE) are derived along with the outage probability. Moreover, we derive closed-form expressions for them in the asymptotic regime. Based on our derivations, insightful investigation shows the existence of two distinct outage probability and ABER floors that depends on the backhaul reliability levels, number of transmitters, and ratio of the transmit power of the transmitters to that of the interferers. These analytical results are validated using link-level simulations.
- It is verified that system configuration parameters, channel parameters, safety zone size, and the transmit power ratio of the transmitters to the interferers determine the convergence rate to these performance floors and ceilings; that is, this convergence rate is proportional to the conventional diversity gain. It is also verified that the high-transmit power offset per 3-dB units [25] is zero independent of all the considered parameters of the proposed system.

Related works:

- The paper [7] assumes an unreliable backhaul link between the relays and the destination in a cooperative relay network. With a nonergodic link failure, this paper investigates the broadcast coding and distributed source coding techniques including distributed compression.
- The paper [19] derives an analytical expression for the outage probability of a finite-sized network under Nakagami-m fading without considering node cooperation. Comparing with this work, we analytically incorporate node cooperation and unreliable backhaul, which are two key design features influencing the performance of many wireless systems. Thus, our work can be viewed as an extension of [19] since we analytically treat the joint impact of node cooperation, backhaul reliability and co-channel interference on the system performance. Moreover, unlike [19], we also provide asymptotic results that verify the existence of performance limits, and identify the impact of key parameters on asymptotic performance.
- The paper [20] derives the outage probability in arbitrarily-shaped finite wireless networks. For a finite number of nodes distributed at random inside a given finite region, this paper investigates the impact of the fading channel and the shape of the region on the outage probability. However, this paper implicitly assumes a completely perfect backhaul without node cooperation.
- The paper [22] considers the backhaul link failure probability (LFP) in the formation of an equivalent system channel matrix. The LFP is determined by the outage probability of the backhaul link. Based on the equivalent channel matrix, this paper mainly investigates the empirical ergodic capacity without its asymptotic analysis. However, this paper does not include interference in the system model.

The rest of the paper is organized as follows. In Section II, we first detail the system and channel model of the proposed system. Derivation of the cumulative distribution function (CDF) of the spatially averaged SINR (SA-SINR) in heterogeneous system and channel parameters is provided in Section III. Performance analysis of the considered system in homogeneous system and channel parameters is presented in Section IV. Simulation results are presented in Section V and conclusions are drawn in Section VI.

Notation: $F_{\varphi}(\cdot)$ and $f_{\varphi}(\cdot)$ respectively denote the CDF and the probability density function (PDF) of the random variable (RV) φ; $E\{\cdot\}$ denotes expectation. In addition, $\binom{n_1}{n_2} \triangleq \frac{n_1!}{n_2!(n_1-n_2)!}$ denotes the binomial coefficient. Additional notation used in this paper is summarized in Table 1.

TABLE I
NOTATION USED IN THIS PAPER

Notation	Description
K	Number of transmitters
M	Number of interferers
p_k	Reliability of the kth backhaul
h_k	Wireless channel from TX_k to the receiver
m_k,n_k	Shape and scale of the gamma distribution, $\lvert h_k\rvert^2 \sim \mathrm{Ga}(m_k, n_k)$
α_k	Pathloss over the channel h_k
$d_{k,R}$	Distance from the TX_k to the receiver
g_i	Wireless channel from the ith interferer to the receiver
$\tilde{m}_i$,$\tilde{n}_i$	Shape and scale of the gamma distribution, $\lvert g_i\rvert^2 \sim \mathrm{Ga}(\tilde{m}_i, \tilde{n}_i)$
$\tilde{\alpha}_i$	Pathloss over the channel g_i
$\tilde{d}_{i,R}$	Distance from the ith interferer to the receiver
ϵ	Pathloss exponent
P	Transmit power at the transmitters
$P_{I,i}$	Transmit power at the ith interferer with $P_{I,i} = \chi_{I,i}P$
$r_{\max}$	Radius for the communication range
$r_{\min}$	Radius for the safety zone with $r_{\min} = \chi_r r_{\max}$

II. System and Channel Model

Fig. 1 shows the block diagram of the considered fixed-sized centralized cooperative system, in which a CU connected to the core network; K single antenna transmitters are connected to the CU via unreliable backhaul links; one receiver (RX) is connected with K transmitters $\{\mathrm{TX}_1, ..., \mathrm{TX}_K\}$ via wireless channels, $\{h_1, \ldots, h_K\}$. We use the orthogonal frequency division multiple access (OFDMA) as the transmission scheme in the downlink, where a cluster of K transmitters send a common message to the receiver over the same time-frequency resource block. In the communication range of the receiver,

[1]The term *backhaul reliability* can be used to model operating conditions that cause a radio link failure [7], [23] due to network congestion, delay, lost radio interface synchronization, and hardware imperfection. Without cooperation between transmitters, a backhaul reliability model is somewhat similar to that of the slotted ALOHA medium access control (MAC) protocol, in which a source only transmits with probability P_{tx} independently of other nodes in a particular time slot, whereas defer its transmission with probability $1 - P_{\mathrm{tx}}$ [24].

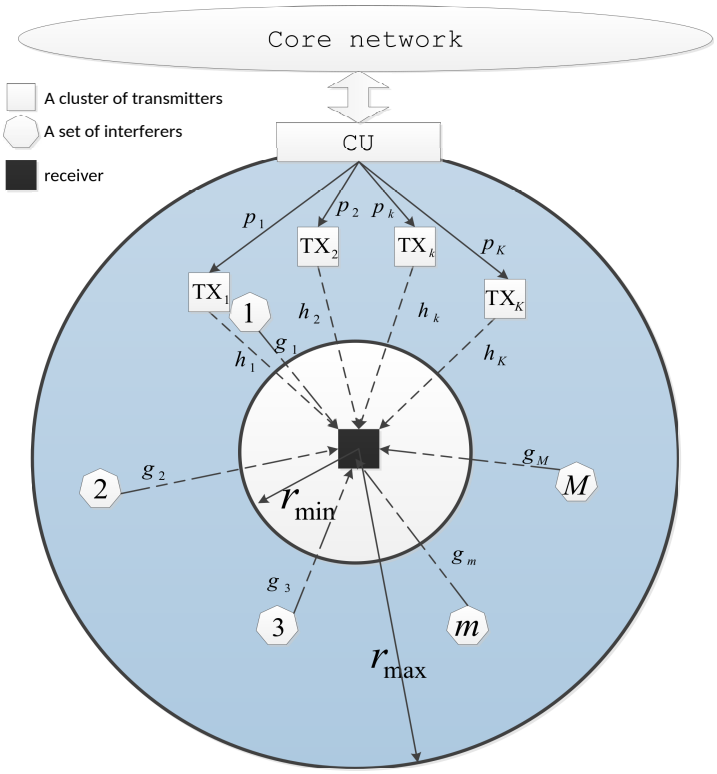

Fig. 1. Block diagram of the considered fixed-sized system with the safety zone and multiple interferers inside of the communication range of the receiver. The safety zone is defined by the radius of the circle, $r_{\min}$.

which is specified by an outer radius $r_{\max}$, M interferers are assumed to coexist with these nodes. Furthermore, these interferers are uniformly distributed in this communication range. For this system, we assume the following about the wireless channel, backhaul reliability, and transmission scheme.

- A safety zone [15]–[19] with a radius $r_{\min} \triangleq \chi_r r_{\max}$ with $0 < \chi_r < 1$ is formed around the receiver, so that there is no interference originating from within this safety zone. In this system, we assume that all nodes are equipped with a localization mechanism to estimate their positions (for example, using GPS [17]), and their positions are available to the nodes in the system [2]. Based on this available position information, a network protocol determines a right safety zone before deploying the nodes in a controlled environment.
- The backhaul reliability for transmitter TX_k is given by $\{p_k, \forall k\}$, so that this transmitter successfully decodes the source message sent over its dedicated backhaul link, whereas it is erased with probability $1 - p_k$ due to its unreliable backhaul. These erasures are assumed to be independent across message and follow a Bernoulli process $\mathrm{Bernoulli}(1 - p_k)$.
- Envelopes of a set of channels $\{h_k, \forall k\}$ between the kth transmitter and the receiver undergo Nakagami-m fading. For generality, each of the K channels are allowed to have possibly different Nakagami-m m parameters.
- Envelopes of a set of channels $\{g_i, \forall i\}$ between the ith interferer and the receiver undergo Nakagami-m fading. As for $\{g_i, \forall i\}$, different Nakagami-m m parameters are considered taking into account different fading conditions between the interferers and the receiver.
- Non-coherent joint OFDM transmission [29] is employed, thereby obviating the need of channel information at the transmitter and also relaxing the requirement of tight synchronization between cooperating transmitters.
- The transmission symbol x is transmitted from the transmitters. We assume that $E\{x\} = 0$ and $E\{|x|^2\} = 1$. The transmission power at the transmitters is given by P.
- The transmission power and the channel from the ith interferer to the receiver are, respectively, denoted by $P_{I,i}$ and g_i, with the path loss over this channel denoted by $\tilde{\alpha}_i$. Also, we assume that the transmission symbols from the interferers, $\{\tilde{x}_i, \forall i\}$, have $E\{\tilde{x}_i\} = 0, \forall i$, $E\{|\tilde{x}_i|^2\} = 1, \forall i$, $E\{\tilde{x}_i \tilde{x}_j^*\} = \delta(i-j), \forall i, j$ with $i \neq j$, and $E\{x\tilde{x}_i^*\} = 0, \forall i$, where $\delta(\cdot)$ denotes the Dirac delta function.

Based on the above channel and transmission scheme, the instantaneous SINR is defined by [29]

$$\lambda = \frac{\sum_{k=1}^{K} \frac{P\alpha_k \mathbb{I}_k |h_k|^2}{\sigma_n^2}}{\sum_{i=1}^{M} \frac{P_{I,i}\tilde{\alpha}_i |g_i|^2}{\sigma_n^2} + 1} \triangleq \frac{S}{N+1} \tag{1}$$

where we assume the receiver noise to be zero-mean additive white complex Gaussian with variance σ_n^2. P and $P_{I,i}$ denote transmit powers at the transmitters and at the ith interferer, respectively. To model the backhaul reliability, we use an indicator function as

$$P_r(\mathbb{I}_k = 1) = p_k \text{ and } P_r(\mathbb{I}_k = 0) = 1 - p_k. \tag{2}$$

We also define the aggregate signal power $S \triangleq \sum_{k=1}^{K} S_k$, where $S_k \triangleq \frac{P\alpha_k \mathbb{I}_k |h_k|^2}{\sigma_n^2}$ denotes the normalized instantaneous received signal power from the kth transmitter. We also define the aggregate interference power $N \triangleq \sum_{i=1}^{M} N_i$, with $N_i \triangleq \frac{P_{I,i}\tilde{\alpha}_i |g_i|^2}{\sigma_n^2}$ denoting the normalized interference power from the ith interferer. The fading envelope of h_k is Nakagami-m distributed with the fading parameter m_k. Similarly, the fading envelope of g_i is Nakagami-m distributed with the fading parameter $\tilde{m}_i$. The pathloss for the channel between two nodes is exponentially decaying as $\alpha_k = d_{k,R}^{-\epsilon}$, where $d_{k,R} \in [\chi_r r_{\max}, r_{\max}]$ is the distance between the kth transmitter and the receiver and ϵ is the path loss exponent. Similarly, we assume $\tilde{\alpha}_i = \tilde{d}_{i,R}^{-\epsilon}$, where $\tilde{d}_{i,R}$ is the distance between the ith interferer and the receiver. Based on (1), we conduct performance analysis in the following sections.

[2]Since the differential GPS (dGPS) system can provide the position estimation in centimeter-level accuracy by applying the double difference between satellites and receivers of the carrier phase measurements [26], the position estimation error is assumed to be negligible in the considered system. The nLOS errors are critical in tracking mobile nodes. To address nLOS errors, many works have been proposed. One approach is to use the time-of-arrival (TOA) between the CU and mobile nodes [27], [28]. Comparing with the time history of the range measurements, we first identify if the measurements come from LOS or nLOS environment. If nNOS is identified at a particular node, construct a LOS propagation model to remove nLOS errors [27]. Applying this approach, the CU can track mobile nodes even in nLOS environment.

III. Derivation of the CDF of the SA-SINR in Heterogeneous System and Channel Parameters

In this section, we will first investigate statistical properties of the SA-SINR for the heterogeneous case.

Definition 1: For the Nakagami-m fading envelope for h_k, $|h_k|^2$ is distributed according to the gamma distribution [30], which is denoted by $|h_k|^2 \sim \mathrm{Ga}(m_k, n_k)$, where m_k is related to the fading severity and defines the shape of the gamma distribution, whereas the scale factor, defined by $n_k = \frac{E\{|h_k|^2\}}{m_k}$ [30], specifies the average fading power [31]. The operating frequency, antenna heights, polarizations, antenna separation distance, and the relative position of the scatters contribute in determining the fading severity [31]. Similarly, we assume $|g_i|^2 \sim \mathrm{Ga}(\tilde{m}_i, \tilde{n}_i)$ with $\tilde{n}_i = \frac{E\{|g_i|^2\}}{\tilde{m}_i}$. For a positive integer value of m_k (we assume this for ease of analysis), the PDF and CDF of $|h_k|^2$ are, respectively, given by

$$f_{|h_k|^2}(x) = \frac{1}{\Gamma(m_k)(n_k)^{m_k}} x^{m_k-1} e^{-\frac{x}{n_k}} \text{ and}$$
$$F_{|h_k|^2}(x) = 1 - \frac{\Gamma_u(m_k, x/n_k)}{\Gamma(m_k)} \tag{3}$$

where $\Gamma(x) \triangleq \int_0^\infty e^{-t} t^{x-1} dt$, and $\Gamma_u(m,x) \triangleq \int_x^\infty e^{-t} t^{m-1} dt$ denotes the upper incomplete gamma function.

From the definition of the signal power S, we can see that S_k is statistically distributed as the product of the Beroulli random process for $\mathbb{I}_k$ and a random process which has the gamma distribution with shape m_k and scale $\eta_k \triangleq \frac{P\alpha_k n_k}{\sigma_n^2}$. However, N_i is distributed as the gamma distribution with shape $\tilde{m}_i$ and scale $\tilde{\eta}_i \triangleq \frac{P_{I,i}\tilde{\alpha}_i \tilde{n}_i}{\sigma_n^2}$. Thus, the expression for the SINR is different from the existing works such as [21], [30], [32], [33] due to an incorporation of the Bernoulli random process in the definition of the SINR. Note that, in the sequel, we will use λ to represent the SINR. Due to different locations of the transmitters and interferers, we assume that $\eta_k \neq \eta_j, \forall k, j$ with $k \neq j$, and $\tilde{\eta}_k \neq \tilde{\eta}_j, \forall k, j$ with $k \neq j$.

Next, the CDF of the SA-SINR is derived in the following theorem.

Theorem 1: For heterogeneous system and channel parameters and an independent Bernoulli random process that models heterogeneous backhaul reliability, the CDF of the SA-SINR is given by (4) at the top of the next page. In (4), $\gamma_l(m_k, x) \triangleq \int_0^x e^{-t} t^{m_k-1} dt$ denotes the lower incomplete gamma function, $Q \triangleq \prod_{k=1}^K (1-p_k)$, and ${}_2F_1(\cdot,\cdot,\cdot,\cdot)$ denotes the Gauss hypergeometric function [34, eq. (9.111)]. In addition, $\Omega_{i,j}$ is defined by

$$\Omega_{i,j} \triangleq \frac{(-1)^{m_i}}{(\eta_i)^{m_i}} \sum_{X(i,j)} \prod_{k=1, k\neq i}^{K} \binom{m_k + k_k - 1}{k_k} \frac{(\eta_k)^{k_k}}{(1-\frac{\eta_k}{\eta_i})^{m_k+k_k}} (\eta_{l_i})^j \triangleq c_{i,j} (\eta_{l_i})^j \tag{5}$$

where $X(i,j)$ denotes a set of K-tuples satisfying the following condition

$$X(i,j) \triangleq \{(k_1, \ldots, k_K) : \sum_{k=1}^K k_k = m_k - j \text{ with } k_i = 0\}.$$

Proof: See Appendix A. ∎

Note that Theorem 1 completely characterizes the SA-SINR of a finite-sized cooperative network. It is applicable to a wide range of scenarios taking into account non-identical Nakagami-m fading links, non-identical backhaul reliability, and any number of cooperating/interfering transmitters. To facilitate the derivation of the performance metrics, we assume homogeneous system and channel parameters in the following section.

IV. Performance Analysis in Homogeneous System and Channel Parameters

In this section, we will compute the outage probability via the derived CDF of the instantaneous SINR. We assume $m = m_k, \forall k$, $\eta = \eta_k, \forall k$, $\alpha = \alpha_k, \forall k$, $\mathbb{I} = \mathbb{I}_k, \forall k$, $p = p_k, \forall k$ for the transmitter relevant parameters. Also, we assume $\tilde{m} = \tilde{m}_k, \forall k$, $\tilde{\eta} = \tilde{\eta}_k, \forall k$, $\tilde{\alpha} = \tilde{\alpha}_k, \forall k$, $P_I = P_{I,k}, \forall k$ and $\chi_I = \chi_{I,k}, \forall k$ for the parameters relevant to the interferers. To further insight on the asymptotic behavior of the system, we derive expressions for the asymptotic outage probability, asymptotic ABER, and asymptotic ASE as well.

Definition 2: Based on the assumptions provided in Section IV, the CDF of the signal power S is given by

$$\begin{aligned} F_S(x) &= Q + Q \sum_{l=1}^{K} \binom{K}{l} (\frac{p}{1-p})^l \frac{1}{\Gamma(ml)} \gamma_l(ml, \frac{x}{\eta}) \\ &= Q + Q \sum_{l=1}^{K} \binom{K}{l} (\frac{p}{1-p})^l \\ &\quad \Big(1 - e^{-\frac{x}{\eta}} \sum_{m'=0}^{ml-1} \frac{1}{\Gamma(m'+1)} (\frac{x}{\eta})^{m'}\Big) \end{aligned} \tag{6}$$

where a finite series representation of the lower incomplete gamma function [34, eq. (8.352.6)] is used. By using (A.5), we can readily derive (6).

According to the properties of the gamma distribution, the distribution of the interference power is given by $N \sim \mathrm{Ga}(\tilde{m}M, \tilde{\eta})$.

A. Outage Probability Analysis

To predict the quality of service of the proposed system over Nakagami fading channels, we first investigate the outage probability. It is defined as the probability that the SINR falls below a given threshold θ, i.e.,

$$O_{\mathrm{out}}(\theta) \triangleq Pr(\lambda \leq \theta) = F_\lambda(\theta) \tag{7}$$

which is the special case of Theorem 1.

Applying the similar procedure as used in Appendix A, especially, using (6) instead of (A.5) in the computation of (A.7), the outage probability is given in the following corollary.

Corollary 1: The outage probability at a fixed SINR threshold θ is given in (8) at the top of the next page.

Proof: According to the derivation of Theorem 1, this corollary can be readily derived. This corollary shows the effects of reliability of the backhauls on the outage probability. ∎

$$F_\lambda(x)=Q\Bigg(1+\sum_{k=1}^{K}\sum_{l_1}^{K-k+1}\sum_{l_2=l_1+1}^{K-k+2}\cdots\sum_{l_k=l_{k-1}+1}^{K}\Big(\prod_{n=1}^{k}\frac{p_{l_n}}{(1-p_{l_n})}\Big)\sum_{i=1}^{k}\sum_{j=1}^{m_i}\frac{\Omega_{i,j}(-1)^j}{\Gamma(j)}\Big(1-e^{-x/\eta_{l_i}}\sum_{p=0}^{j-1}\big(\frac{x}{\eta_{l_i}}\big)^p$$
$$\sum_{q=0}^{p}\sum_{\substack{j_1,j_2,\cdots,j_M\\ j_1+\cdots+j_M=q}}^{q}\frac{1}{(p-q)!}\prod_{t=1}^{M}\frac{1}{j_t!}\frac{\Gamma(j_t+\tilde{m}_t)}{\Gamma(\tilde{m}_t)(\frac{P_{I,t}\tilde{n}_t}{\sigma_n^2})^{\tilde{m}_t}}\frac{2\Big(\frac{x}{\eta_{l_i}}\Big)^{-(j_t+\tilde{m}_t)}\frac{1}{\tilde{m}_t+2/\epsilon}(r_{\max}^{\epsilon\tilde{m}_t+2})}{\epsilon r_{\max}^2[1-\chi_r^2]}$$
$$\big[{}_2F_1\big(\tilde{m}_t+\frac{2}{\epsilon},j_t+\tilde{m}_t;\tilde{m}_t+\frac{2}{\epsilon}+1;-\frac{r_{\max}^{\epsilon}\tilde{\eta}_{l_i}\sigma_n^2}{xP_{I,t}\tilde{n}_t}\big)-$$
$$\chi_r^{\epsilon\tilde{m}_t+2}{}_2F_1\big(\tilde{m}_t+\frac{2}{\epsilon},j_t+\tilde{m}_t;\tilde{m}_t+\frac{2}{\epsilon}+1;-\frac{\chi_r^{\epsilon}r_{\max}^{\epsilon}\tilde{\eta}_{l_i}\sigma_n^2}{xP_{I,t}\tilde{n}_t}\big)\big]\Big)\Bigg). \tag{4}$$

$$O_{\text{out}}(\theta)=Q+Q\sum_{l=1}^{K}\binom{K}{l}\big(\frac{p}{1-p}\big)^l-\frac{2Q}{\epsilon r_{\max}^2[1-\chi_r^2]}\sum_{l=1}^{K}\binom{K}{l}\big(\frac{p}{1-p}\big)^l e^{-\frac{\theta}{\eta}}$$
$$\sum_{m'=0}^{ml-1}\big(\frac{\theta}{\eta}\big)^{m'}\sum_{n=0}^{m'}\binom{m'}{n}\frac{\Gamma(\tilde{m}M+n))(\tilde{\eta})^n}{\Gamma(\tilde{m}M)\Gamma(m+1)(\tilde{m}M+2/\epsilon)}\big(\frac{P_I}{\mu}\theta\big)^{-(\tilde{m}M+n)}(r_{\max})^{\epsilon\tilde{m}M+2}$$
$$\Big[{}_2F_1\big(\tilde{m}M+\frac{2}{\epsilon},\tilde{m}M+n;\tilde{m}M+\frac{2}{\epsilon}+1;-\frac{r_{\max}^{\epsilon}\mu P}{\theta P_I}\big)-$$
$$\chi_r^{\epsilon\tilde{m}M+2}{}_2F_1\big(\tilde{m}M+\frac{2}{\epsilon},\tilde{m}M+n;\tilde{m}M+\frac{2}{\epsilon}+1;-\frac{\chi_r^{\epsilon}r_{\max}^{\epsilon}\mu P}{\theta P_I}\big)\Big],\ \text{with}\ \mu\stackrel{\triangle}{=}\frac{d^{-\epsilon}n}{\tilde{n}}. \tag{8}$$

Corollary 2: When the interference power is proportional to the transmit power P, an outage probability floor exists due to interference.

Proof: The existence of the outage probability floor follows immediately from Corollary 1. Upon applying $\frac{P}{P_I}=\kappa$ into (8), we obtain (9) at the top of the next page. In (9), $B(\cdot,\cdot)$ denotes the beta function [34, eq. (8.384.1)]. Note that only a dominating term is extracted from (8) in the derivation of (9). For a particular scenario, where the interference power is proportional to the transmit power, this corollary shows that interference specified by system configuration parameters, channel fading parameters, and backhaul link reliability jointly determine the outage probability floor. ∎

Corollary 3: For a fixed interference power P_I, the asymptotic outage probability as the transmit power $P\to\infty$ is given by

$$O_{2,\text{out}}^{\infty}(\theta)=Q. \tag{10}$$

Proof: See Appendix B. ∎

This corollary shows the existence of another outage probability floor, which is mainly determined by reliability of the backhaul links. As opposed to Corollary 2, this outage probability floor is independent of interference. From Corollaries 2 and 3, we can see the following asymptotic behavior of the system in terms of the outage probability:

- As K increases, a lower outage probability can be obtained. Also, the outage probability converges to $O_{2,\text{out}}^{\infty}(\theta)$ at a faster rater as m increases.
- As either M or $\tilde{m}$ increases, outage happens more frequently due to a greater interference when the interference power is proportional to the transmit power. When the interference power is fixed, a slower rate is obtained converging to $O_{2,\text{out}}^{\infty}(\theta)$ due to a greater interference from the interferers.
- The size of the communication range of the receiver also affects $O_{1,\text{out}}^{\infty}(\theta)$ and the rate converging to $O_{2,\text{out}}^{\infty}(\theta)$. As either $r_{\max}$ or χ_r increases, a lower outage probability and a faster rate converging to $O_{2,\text{out}}^{\infty}(\theta)$ can be achieved due to reduced interference.
- Due to existence of two distinct outage floors, an asymptotic diversity gain [35] cannot be achieved.

B. Average Bit Error Rate Analysis

In this subsection, we derive the ABER for Binary Phase-Shift Keying (BPSK) modulation based on the distribution of λ, which can be implied from (8). The ABER is given as [36]

$$S_b=\frac{1}{2\sqrt{\pi}}\int_0^{\infty}x^{-1/2}F_\lambda(x)e^{-x}dx. \tag{11}$$

Now applying $F_\lambda(x)$ into (11), yields the following

$$S_b=\frac{Q}{2}+\frac{Q}{2}\sum_{l=1}^{K}\binom{K}{l}\big(\frac{p}{1-p}\big)^l-\tilde{S}_b \tag{12}$$

where

$$\tilde{S}_b\stackrel{\triangle}{=}\frac{Q}{\sqrt{\pi}\epsilon r_{\max}^2[1-\chi_r^2]}\sum_{l=1}^{K}\binom{K}{l}\big(\frac{p}{1-p}\big)^l$$
$$\sum_{m'=0}^{ml-1}\sum_{n=0}^{m'}\binom{m'}{n}\frac{\big(\frac{1}{\eta}\big)^{m'}(1+\frac{1}{\eta})^{-1}(\tilde{\eta})^n\big(\frac{P_I}{\mu P}\big)^{-(m'-1/2)}}{\Gamma(\tilde{m}M)\Gamma(m'+1)}$$

$$O_{1,\text{out}}^{\infty}(\theta)=1-\frac{2Q}{\epsilon r_{\max}^{2}[1-\chi_r^2]}\sum_{l=1}^{K}\binom{K}{l}(\frac{p}{1-p})^{l}\sum_{m'=0}^{ml-1}\frac{\left(\kappa\mu\right)^{(\tilde{m}M)}\theta^{-\tilde{m}M}(r_{\max})^{\epsilon\tilde{m}M+2}}{(\tilde{m}M+m')B(\tilde{m}M,m'+1)(\tilde{m}M+2/\epsilon)}$$
$$\Bigg[{}_2F_1\big(\tilde{m}M+\frac{2}{\epsilon},\tilde{m}M+m';\tilde{m}M+\frac{2}{\epsilon}+1;-\frac{r_{\max}^{\epsilon}\kappa\mu}{\theta}\big)-$$
$$\chi_r^{\epsilon\tilde{m}M+2}{}_2F_1\big(\tilde{m}M+\frac{2}{\epsilon},\tilde{m}M+m';\tilde{m}M+\frac{2}{\epsilon}+1;-\frac{\chi_r^{\epsilon}r_{\max}^{\epsilon}\kappa\mu}{\theta}\big)\Bigg]. \quad (9)$$

$$r_{\max}^{-\epsilon(C_a)}\Bigg[G_{3,2}^{2,2}\Big(\begin{matrix}a_1,a_2,a_3\\b_1,b_2\end{matrix}\Big|\frac{P_I}{r_{\max}^{\epsilon}\mu P(1+\frac{1}{\eta})}\Big)-$$
$$\chi_r^{-\epsilon(C_a)}G_{3,2}^{2,2}\Big(\begin{matrix}a_1,a_2,a_3\\b_1,b_2\end{matrix}\Big|\frac{P_I}{\chi_r^{\epsilon}r_{\max}^{\epsilon}\mu P(1+\frac{1}{\eta})}\Big)\Bigg] \quad (13)$$

with $a_1\overset{\triangle}{=}1-\tilde{m}M-n+m'-1/2$, $a_2\overset{\triangle}{=}0$, $a_3\overset{\triangle}{=}2/\epsilon-n+\tilde{m}+1/2$, $b_1\overset{\triangle}{=}2/\epsilon-n+m'-1/2$, and $b_2\overset{\triangle}{=}m'-1/2$. Also, $C_a\overset{\triangle}{=}n-\tilde{m}-2/\epsilon+1/2$ and $G_{p,q}^{m,n}\Big(\begin{matrix}a_1,\cdots,a_p\\b_1,\cdots,b_q\end{matrix}\Big|\cdot\Big)$ denotes the MeijerG function [34, eq. (9.301)]. A derivation of (12) is provided in Appendix C.

Corollary 4: The asymptotic diversity gain cannot be achieved in the considered system.

Proof: As $z\to 0$, $G_{p,q}^{m,n}\Big(\begin{matrix}a_1,\cdots,a_n,a_{n+1},\cdots,a_p\\b_1,\cdots,b_m,b_{m+1},\cdots,b_q\end{matrix}\Big|z\Big)\propto z^{\beta}$, where $\beta=\min(b_1,\ldots,b_m)$ [37, Section 5.4.1]. Thus, as $P\to\infty$, we have the corresponding asymptotic expression for $\tilde{S}_b$ provided in (14) at the top of the next page. ∎

Note that (14) verifies that the asymptotic ABER is independent of P.

Corollary 5: Depending on whether the interference power is proportional to the transmit power or not, two distinct asymptotic ABER floors exist.

Proof: As in the derivation of Corollary 2, we can easily find $S_{1,b}^{\infty}$ when the interference power is proportional to the transmit power, and $S_{2,b}^{\infty}$ when the interference power is fixed. Especially, since $F_{2,\lambda}^{\infty}(x)=Q$ as $P\to\infty$, we can see $S_{2,b}^{\infty}=\frac{Q}{2}$. ∎

Note that from Corollary 5, we can see a similar asymptotic ABER behavior as that of the asymptotic outage probability. Since two distinct ABER floors dominate the asymptotic ABER in the high transmit power region, a diversity gain is, in general, not achievable with unreliable backhaul links and/or with interferers within the communication range of the receiver. However, in the medium transmit power region, a different rate converging to these floors can be obtained. In general, the ABER improves with the number of transmitters due to an increased signal power at the receiver. Moreover, the ABER reduces as the communication range of the receiver is increased for a fixed number of interferers. This is because the aggregate interference power at the receiver is reduced due to higher path loss.

C. Average Spectral Efficiency Analysis

In this subsection, we investigate the ASE of the proposed network system. With the available CDF, $F_{\lambda}(x)$, the ASE is defined as [36]

$$R=\frac{1}{\log(2)}\int_0^{\infty}\frac{1-F_{\lambda}(x)}{1+x}dx. \quad (15)$$

Although we have the expression for $F_{\lambda}(x)$, it is infeasible to find an exact ASE. Thus, an upper bound on the ASE will be derived to see the performance behavior of the system.

Theorem 2: An upper bound on the ASE of the proposed system is given by (16) at the top of the next page. In (16), we have defined $C_b\overset{\triangle}{=}n-\tilde{m}-2/\epsilon$.

Proof: See Appendix D. ∎

From Theorem 2, the following corollary can be immediately derived.

Corollary 6: The high-transmit power slope and the power offset per 3-dB units are, respectively, given by

$$S_{\infty}=\log_2\Big(\frac{2\Theta(1-p)^{K-1}Kp\alpha n}{\epsilon\Gamma(\tilde{m}M)}\Big)\text{ and}$$
$$L_{\infty}=0 \quad (17)$$

where Θ is a constant in approximating the MeijerG function. Equation (17) shows that the power offset is not affected by the channel and system configuration parameters.

Proof: We again use the asymptotic expression for the MeijerG function, so that

$$R^{\text{up}}=\log_2\Big(1+\int_0^{\infty}(1-F_{\lambda}(x))dx\Big)$$
$$=\log_2\Big(1+\frac{2\Theta QK\eta}{\epsilon\Gamma(\tilde{m}M)}(\frac{p}{1-p})\Big). \quad (18)$$

Now replacing definitions on terms in (18), (18) is given by $R^{\text{up}}=\log_2(1+\frac{2\Theta(1-p)^{K-1}KpP\alpha n}{\epsilon\Gamma(\tilde{m}M)\sigma_n^2})$, which is in turn given by $R^{\text{up}}\approx\log_2(\frac{2\Theta(1-p)^{K-1}KpP\alpha n}{\epsilon\Gamma(\tilde{m}M)\sigma_n^2})$. Thus, $S_{\infty}=\lim\frac{R^{\text{up}}}{\log_2(P/\sigma_n^2)}=\log_2\Big(\frac{2\Theta(1-p)^{K-1}Kp\alpha n}{\epsilon\Gamma(\tilde{m}M)}\Big)$ and $L_{\infty}=\lim\Big(\log_2(P/\sigma_n^2)-\frac{R^{\text{up}}}{S_{\infty}}\Big)=0$. ∎

Corollary 7: When the interference power is proportional to the transmit power, the ASE ceiling exists due to interference, which is provided by (19) at the top of the next page. Note that (19) shows that as in line with Corollary 2, the system configuration parameters, channel fading parameters, and the backhaul reliability jointly determine the asymptotic ASE ceiling. Note that to derive a more tight ASE ceiling, we have used a different approximation which is described in Appendix

$$\tilde{S}_b \propto \frac{Q}{\sqrt{\pi}\epsilon r_{\max})^2[1-\chi_r^2]} K\Big(\frac{p}{1-p}\Big) \frac{(1+\frac{1}{\eta})^{-1}\big(\frac{P_I}{\mu P}\big)^{1/2}(r_{\max})^{2-\epsilon/2}}{\Gamma(\tilde{m}M)}$$
$$\Bigg[G_{3,2}^{2,2}\Big(\begin{array}{c} 1/2-\tilde{m}M, 0, 2/\epsilon+1/2 \\ 2/\epsilon-1/2, -1/2 \end{array} \Big| \frac{P_I}{r_{\max}^{\epsilon}\mu P(1+\frac{1}{\eta})}\Big) -$$
$$\chi_r^{2-\epsilon/2} G_{3,2}^{2,2}\Big(\begin{array}{c} 1/2-\tilde{m}M, 0, 2/\epsilon+1/2 \\ 2/\epsilon-1/2, -1/2 \end{array} \Big| \frac{P_I}{\chi_r^{\epsilon} r_{\max}^{\epsilon}\mu P(1+\frac{1}{\eta})}\Big)\Bigg]$$
$$= -\frac{Q}{\sqrt{\pi}\epsilon} K\Big(\frac{p}{1-p}\Big) \frac{(1+\frac{1}{\eta})^{-1/2}}{\Gamma(\tilde{m}M)} \approx -\frac{Q}{\sqrt{\pi}\epsilon} \frac{Kp}{\Gamma(\tilde{m}M)(1-p)}. \tag{14}$$

$$R^{\text{up}} = \log_2\Big(1+\int_0^{\infty}(1-F_{\lambda}(x))dx\Big)$$
$$= \log_2\Bigg(1+\frac{2Q}{\epsilon r_{\max}^2[1-\chi_r^2]} \sum_{l=1}^{K}\binom{K}{l}(\frac{p}{1-p})^l \sum_{m'=0}^{ml-1}\sum_{n=0}^{m'}\binom{m'}{n} \frac{\big(\frac{1}{\eta}\big)^{m'-1}(\tilde{\eta})^n\big(\frac{P_I}{\mu P}\big)^{-(m')}}{\Gamma(\tilde{m}M)\Gamma(m'+1)}$$
$$r_{\max}^{-\epsilon(C_b)}\Bigg[G_{3,2}^{2,2}\Big(\begin{array}{c} \tilde{a}_1, \tilde{a}_2, \tilde{a}_3 \\ \tilde{b}_1, \tilde{b}_2 \end{array} \Big| \frac{\eta P_I}{r_{\max}^{\epsilon}\mu P}\Big) - \chi_r^{-\epsilon(C_b)} G_{3,2}^{2,2}\Big(\begin{array}{c} \tilde{a}_1, \tilde{a}_2, \tilde{a}_3 \\ \tilde{b}_1, \tilde{b}_2 \end{array} \Big| \frac{\eta P_I}{\chi_r^{\epsilon} r_{\max}^{\epsilon}\mu P}\Big)\Bigg]\Bigg). \tag{16}$$

$$R_1^{\infty} = \frac{2Q}{\log(2)\epsilon r_{\max}^2[1-\chi_r^2]} \sum_{l=1}^{K}\binom{K}{l}(\frac{p}{1-p})^l \sum_{m'=0}^{ml-1} \frac{1}{\Gamma(\tilde{m}M+m'+1)B(\tilde{m}M, m'+1)} \big(\kappa\mu\big)^{(\tilde{m}M)}$$
$$r_{\max}^{\epsilon\tilde{m}M+2}\Bigg[G_{3,3}^{3,2}\Big(\begin{array}{c} 1, \tilde{m}M, \tilde{m}M+2/\epsilon+1 \\ \tilde{m}M+2/\epsilon, \tilde{m}M+m', \tilde{m}M \end{array} \Big| \frac{1}{r_{\max}^{\epsilon}\kappa\mu}\Big) -$$
$$\chi_r^{\epsilon\tilde{m}M+2} G_{3,3}^{3,2}\Big(\begin{array}{c} 1, \tilde{m}M, \tilde{m}M+2/\epsilon+1 \\ \tilde{m}M+2/\epsilon, \tilde{m}M+m', \tilde{m}M \end{array} \Big| \frac{1}{\chi_r^{\epsilon} r_{\max}^{\epsilon}\kappa\mu}\Big)\Bigg]. \tag{19}$$

E. When the interference power is fixed, the ASE is seen to be proportional to the transmission power P as in (18).

V. Simulation Results

In the simulations, we use BPSK modulation. We assume $\epsilon = 4$ for all the channels in the considered system. The following various simulation scenarios are considered to verify the performance of the proposed network system. We use the normalized $r_{\min}$ and $P_{I,i},\ \forall i$ with respect to $r_{\max}$ and P; that is, $r_{\min} = \chi_r r_{\max}$ and $P_{I,i} = \chi_{I,i} P$ with $0 < \chi_r < 1$ and $0 < \chi_{I,i} < 1,\ \forall i$.

- E_0 : $K = 3$ with $m_k = \{1,2,3\}$, $p_k = \{0.99, 0.98, 0.97\}$, $\tilde{m}_i = \{1,2,1\}$, $\chi_{I,i} = 0.01, \forall i$, $r_{\max} = 1$, $\chi_r = 0.1$.
- E_1 : $K = 3$ with $m_k = \{2,3,4\}$, $p_k = \{0.99, 0.98, 0.97\}$, $\tilde{m}_i = \{1,2,1\}$, $\chi_{I,i} = 0.01, \forall i$, $r_{\max} = 1$, $\chi_r = 0.1$.
- E_2 : $K = 3$ with $m_k = \{2,3,4\}$, $p_k = \{0.99, 0.98, 0.97\}$, $\tilde{m}_i = \{2,3,4\}$, $\chi_{I,i} = 0.01, \forall i$, $r_{\max} = 1$, $\chi_r = 0.1$.
- E_3 : $K = 3$ with $m_k = \{2,3,4\}$, $p_k = \{0.99, 0.98, 0.97\}$, $\tilde{m}_i = \{1,2,1\}$, $\chi_{I,i} = 0.1, \forall i$, $r_{\max} = 1$, $\chi_r = 0.1$.
- E_4 : $K = 3$ with $m_k = \{2,3,4\}$, $p_k = \{0.99, 0.98, 0.97\}$, $\tilde{m}_i = \{1,2,1\}$, $\chi_{I,i} = 0.01, \forall i$, $r_{\max} = 1$, $\chi_r = 0.3$.
- E_5 : $K = 3$ with $m_k = \{2,3,4\}$, $p_k = \{0.99, 0.98, 0.97\}$, $\tilde{m}_i = \{1,2,1\}$, $\chi_{I,i} = 0.01, \forall i$, $r_{\max} = 3$, $\chi_r = 0.1$.
- E_6 : $K = 4$ with $m_k = \{2,3,4,2\}$, $p_k = \{0.99, 0.98, 0.97, 0.96\}$, $\tilde{m}_i = \{1,2,1\}$, $\chi_{I,i} = 0.01, \forall i$, $r_{\max} = 3$, $\chi_r = 0.1$.
- E_7 : $K = 3$ with $m = 2$, $p = 0.99$, $\tilde{m} = 2$, $\chi_I = 0.1$, $r_{\max} = 1$, $\chi_r = 0.3$.
- E_8 : $K = 3$ with $m = 3$, $p = 0.99$, $\tilde{m} = 2$, $\chi_I = 0.1$, $r_{\max} = 1$, $\chi_r = 0.3$.
- E_9 : $K = 3$ with $m = 3$, $p = 0.99$, $\tilde{m} = 3$, $\chi_I = 0.1$, $r_{\max} = 1$, $\chi_r = 0.3$.
- E_{10} : $K = 3$ with $m = 3$, $p = 0.99$, $\tilde{m} = 2$, $\chi_I = 0.1$, $r_{\max} = 3$, $\chi_r = 0.1$.
- E_{11} : $K = 3$ with $m = 2$, $p = 0.5$, $\tilde{m} = 2$, $\chi_I = 0.1$, $r_{\max} = 1$, $\chi_r = 0.3$.
- E_{12} : $K = 2$ with $m = 2$, $p = 0.5$, $\tilde{m} = 2$, $\chi_I = 0.1$, $r_{\max} = 1$, $\chi_r = 0.3$.
- E_{13} : $K = 3$ with $m = 2$, $p = 0.99$, $\tilde{m} = 2$, $\chi_I = 0.1$, $r_{\max} = 1$, $\chi_r = 0.01$.

- F_1 : $K = 3$ with $m_k = \{2,3,4\}$, $p_k = \{0.99, 0.98, 0.97\}$, $\tilde{m}_i = \{1,2,1\}$, $\chi_{I,i} = 0.01, \forall i$, $r_{\max} = 1$, $\chi_r = 0$.
- F_2 : $K = 3$ with $m_k = \{2,3,4\}$, $p_k = \{0.99, 0.98, 0.97\}$, $\tilde{m}_i = \{1,2,1\}$, $\chi_{I,i} = 0.01, \forall i$, $r_{\max} = 3$, $\chi_r = 0$.
- F_3 : $K = 4$ with $m_k = \{2,3,4,2\}$, $p_k = \{0.99, 0.98, 0.97, 0.96\}$, $\tilde{m}_i = \{1,2,1\}$, $\chi_{I,i} = 0.01, \forall i$, $r_{\max} = 3$, $\chi_r = 0$.

Scenarios E_1-E_6 are used for heterogeneous system parameters, whereas E_7-E_{13} are used for homogeneous system parameters. Scenarios F_1-F_3 are same as E_4-E_6 without safety zone.

In the following figures, the curves obtained by actual link simulations are denoted by **Ex**, whereas analytically derived curves are denoted by **An**. Asymptotically obtained curves are denoted by **As**.

A. Outage Probability Analysis

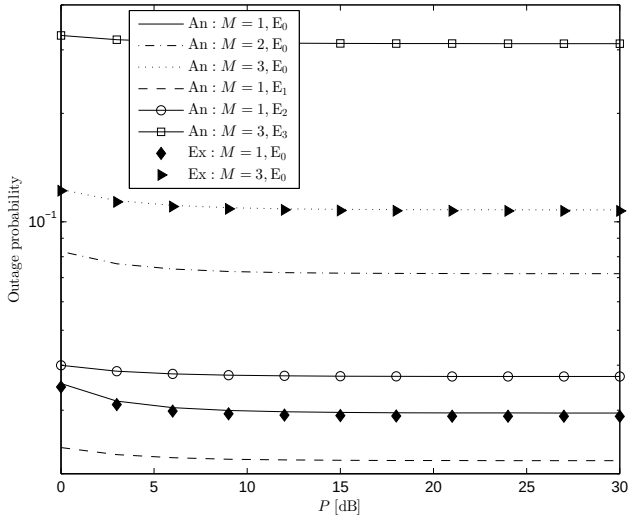

Fig. 2. Outage probability for various simulation scenarios.

In Figs. 2 and 3, we use heterogeneous system parameters. We assume that the interference power is proportional to the transmit power. From Fig. 2, we investigate the effects of the system configurations and channels.

- The effect of the number of interferers: More interference increases the outage probability. For example, $(M = 1, \mathrm{E}_0)$ vs. $(M = 2, \mathrm{E}_0)$.
- The effect of Nakagagami-m m parameter of the signal channel: A greater value of m leads to a lower outage probability since fluctuation of the signal power reduced with a greater value of m. For example, $(M = 1, \mathrm{E}_0)$ vs. $(M = 1, \mathrm{E}_1)$.
- The effect of Nakagagami-m $\tilde{m}$ parameter of the interfering channel: A greater value of $\tilde{m}$ leads to a higher outage probability due to a greater interference. For example, $(M = 1, \mathrm{E}_1)$ vs. $(M = 1, \mathrm{E}_2)$.

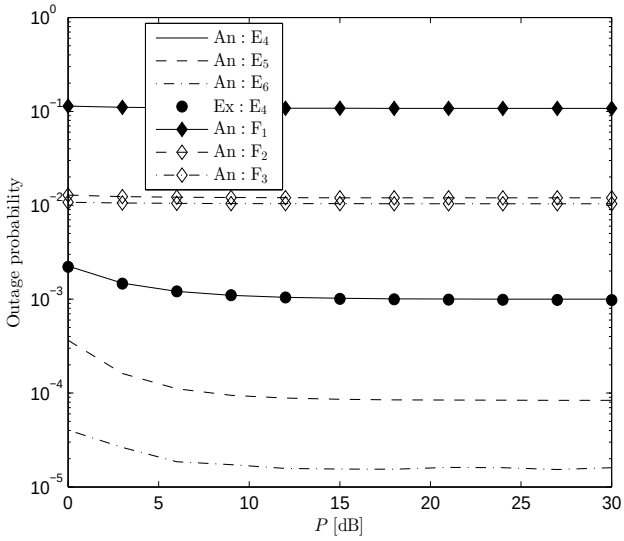

Fig. 3. Outage probability for various simulation scenarios with $M = 3$.

- The effect of the interfering power: As χ_I increases, more frequent outages happen. For example, $(M = 1, \mathrm{E}_2)$ vs. $(M = 1, \mathrm{E}_3)$.
- The effect of the safety zone on the outage probability is significant over the system without forming the safety zone.

For the scenario E_0, we also verified our derived closed form expression for the outage probability for $M = 1$ and $M = 3$. We can see the accuracy of the derived outage probability. We can also see that when the interference power is proportional to the transmit power, the outage probability floor always exists. Interference is responsible for this floor. From Fig. 3, we can see the effects of the communication range and safety zone size on the outage probability. As either χ_r or $r_{\max}$ increases, it can be seen that a lower outage happens due to reduced interference at the receiver. For example, $(M = 3, \mathrm{E}_4)$ vs. $(M = 3, \mathrm{E}_5)$ and $(M = 3, \mathrm{E}_5)$ vs. $(M = 3, \mathrm{E}_6)$.

In Figs. 4 and 5, we assume that the interference power is fixed in identical Nakagami-m fading. From these two figures, we can see the following facts:

- In the scenarios such as E_7, E_8, and E_9, the outage probability approaches the outage probability floor, $O^{\infty}_{2,\mathrm{out}} = (1-p)^K$, independent of M, m, $\tilde{m}$, χ_I, and $(r_{\max}, \chi_r)$ as Corollary 3 verified. Only backhaul link reliability is responsible for the outage probability floor.
- A rate converging to this outage probability floor depends on M, m, $\tilde{m}$, χ_I, and $(r_{\max}, \chi_r)$. As m, $r_{\max}$, or χ_r increases, a faster convergence rate can be obtained, whereas as M, $\tilde{m}$, or χ_I increases, a slower convergence rate can be obtained.

Thus, from Figs. 2-5, we can show the existence of two independent outage probability floors in the considered system, and their dominance in the high transmit power region.

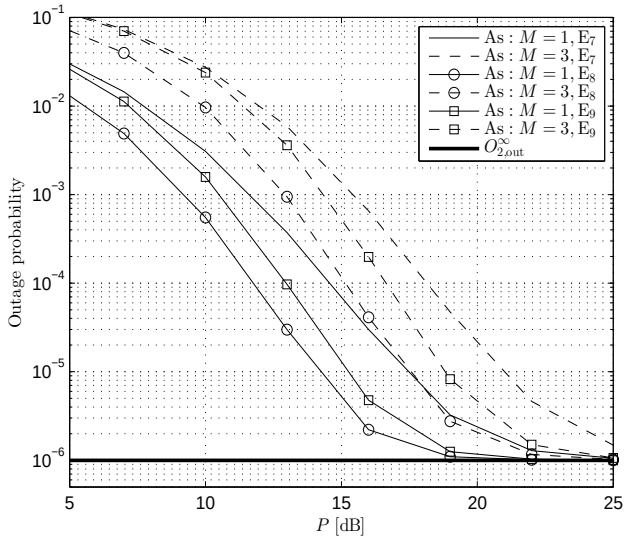

Fig. 4. Outage probability for various simulation scenarios.

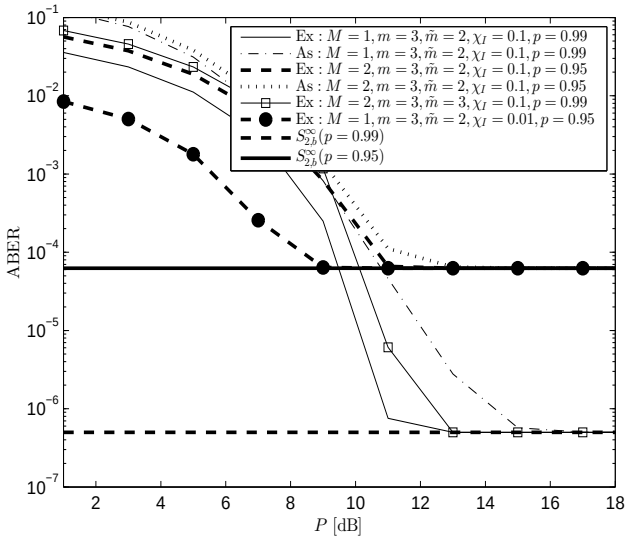

Fig. 6. Average bit error rate for various simulation scenarios with fixed $K = 3$, $r_{\max} = 1$, and $\chi_r = 0.1$.

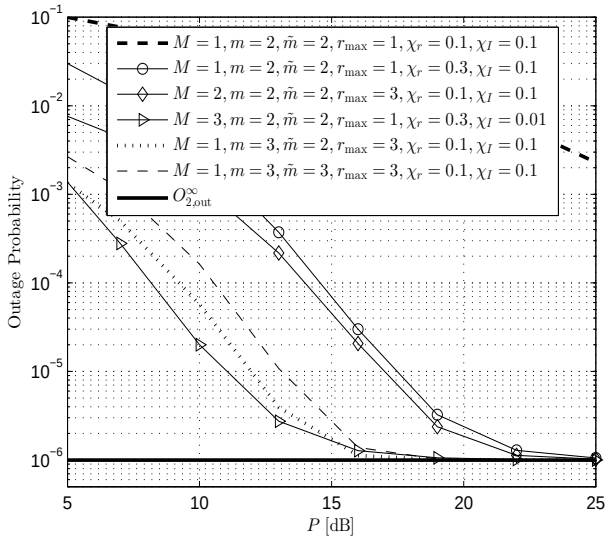

Fig. 5. Outage probability for various simulation scenarios with fixed $K = 3$ and $p = 0.99$.

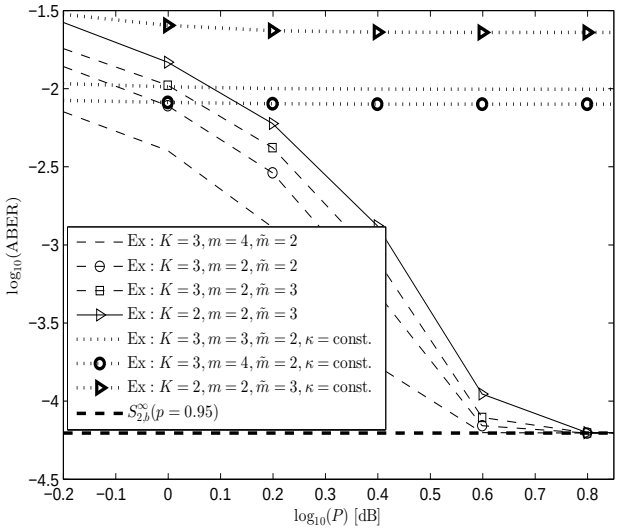

Fig. 7. Analysis of the rate converging to the average bit error rate floor for various scenarios with fixed $M = 1, \chi_I = 0.01$, and $(r_{\max} = 1, \chi_r = 0.1)$.

B. Average Bit Error Rate Analysis

In Fig. 6, we compare the ABER for various scenarios with fixed values of $K = 3$, $r_{\max} = 1$, and $\chi_r = 0.1$. We assume that the interference power is fixed for this figure. For two different backhaul link reliabilities, we can see that as P increases, S_b approaches $S^{\infty}_{2,b} = (1-p)^K/2$, which is mainly determined by the reliability of the backhaul links. As m increases or χ_I decreases, ABER converges to $S^{\infty}_{2,b}$ at a faster rate, whereas a slower convergence to $S^{\infty}_{2,b}$ can be observed when either M or $\tilde{m}$ increases due to greater interference. We also include a curve showing asymptotic ABER behavior. As P increases, differences between the exact ABER and the asymptotic ABER become negligible.

In Fig. 7, we compare converging rate via $\log_{10}(\mathrm{ABER})$ for various scenarios at a particular value of $Q = 1.25 \times 10^{-4}$. We can see that as either m or K increases, a faster convergence to $S^{\infty}_{2,b}$ can be observed when the interference power is fixed. However, when the interference power is proportional to the transmit power, all the considered scenarios result in ABER floors $S^{\infty}_{1,b}$ in the range of $(-0.2, 1.2)$ dBs of P. However, as either m or K increases, it is seen that a lower ABER floor can be obtained.

C. Average Spectral Efficiency Analysis

Fig. 8 shows the ASE for various scenarios. We can observe the following facts:

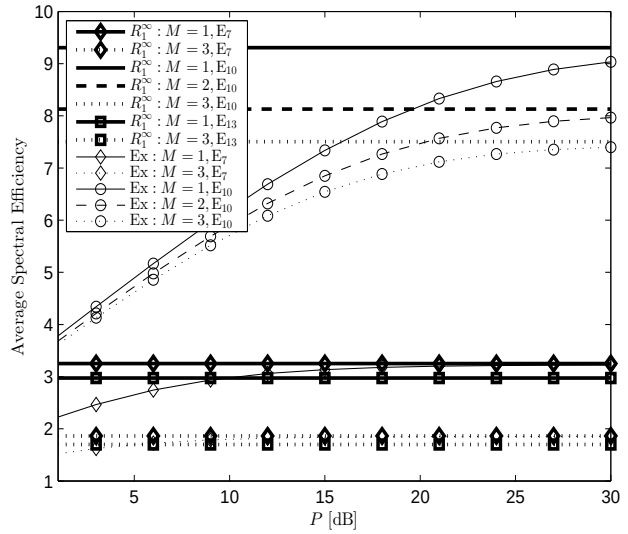

Fig. 8. Average spectral efficiency for various values of M and the interference power proportional to the transmit power.

- When the interference power is proportional to the transmit power, the exact ASE approaches the ASE ceiling R_1^∞ as P increases. Depending on parameters, different ceilings can be obtained as verified by Corollary 7.
- For the same scenario, a greater number of interferers results in a lower ASE due to more interference.
- If we compare scenarios E_7 and E_{10}, it can be seen that a higher ASE can be achieved as m increases.
- If we compare scenarios E_7 and E_{13}, it can be seen that a larger safety zone results in a higher ASE due to reduced interference in the communication range of the receiver.

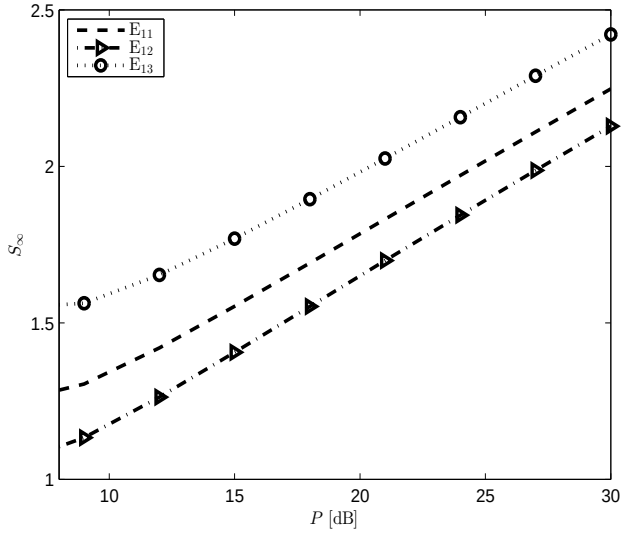

Fig. 9. S_∞ at a fixed interference power and $M = 1$.

In Fig. 9, we show the high-transmit power slope, S_∞ for scenarios, E_{11}, E_{12}, and E_{13} with $M = 1$. We can see that these scenarios have the same S_∞ independent of K, p, and m.

VI. Conclusions

In this paper, a joint impact of aggregate interference from coexisting multiple interferers in the communication range within which the safety zone is formed around the receiver, reliability of the backhaul links, and the size of the communication range has been investigated for the proposed finite-sized cooperative system which connected to the CU via unreliable wireless backhaul links. After deriving the distribution of the spatially averaged SINR at the target receiver in heterogeneous system and channel parameters, we have derived closed-form expressions for the outage probability. To gain further insights into the impact of the backhaul reliability, several system and channel parameters on the performance, an asymptotic analysis has been conducted in the outage probability, ABER, and ASE for homogeneous system and channel parameters. It has been seen that since two intrinsic floors in the outage probability and ABER are dominating in the high transmit power region, a conventional diversity gain is not achievable. Aggregate interference and unreliable backhaul are responsible for these floors. On the other hand, a different rate converging to these floors can be obtained in proportional to the system and channel parameters. Based on the asymptotic ASE, we have shown existence of the ASE ceiling, and verified a zero power offset.

Appendix A: Derivation of Theorem 1

Based on the definition of S, we have

$$S = \sum_{k=1}^{K} S_k = \sum_{k=1}^{K} \mathbb{I}_k \psi_k \tag{A.1}$$

where $\psi_k \overset{\triangle}{=} \frac{P_k \alpha_k |h_k|^2}{\sigma_n^2} \sim \mathrm{Ga}(m_k, \eta_k)$. From the Bernoulli process, the PDF of the RV $\mathbb{I}_k \psi_k$ is given by

$$f_{\mathbb{I}_k \psi_k}(x) = (1 - p_k)\delta(x) + p_k f_{\psi_k}(x) \tag{A.2}$$

where $\delta(\cdot)$ denotes the Dirac delta function. After computing the moment generating function (MGF) of the RV $\mathbb{I}_k \psi_k$, and the partial fraction, we have the following MGF for the RV S

$$M(S) = Q\Bigg(1 + \sum_{k=1}^{K} \sum_{l_1=1}^{K-k+1} \sum_{l_2=l_1+1}^{K-k+2} \cdots \sum_{l_k=l_{k-1}+1}^{K} \Big(\prod_{n=1}^{k} \frac{p_{l_n}}{(1-p_{l_n})}\Big) \sum_{i=1}^{k} \sum_{j=1}^{m_i} \frac{c_{i,j}}{(s + \frac{1}{\eta_{l_i}})^j}\Bigg). \tag{A.3}$$

Now applying the inverse MGF, the PDF of the RV S is obtained as follows:

$$f_S(x) = Q\Big(\delta(x) + \sum_{k=1}^{K} \sum_{l_1=1}^{K-k+1} \sum_{l_2=l_1+1}^{K-k+2} \cdots \sum_{l_k=l_{k-1}+1}^{K} \Big(\prod_{n=1}^{k} \frac{p_{l_n}}{(1-p_{l_n})}\Big) \sum_{i=1}^{k} \sum_{j=1}^{m_i} \frac{c_{i,j}(-1)^j}{\Gamma(j)} x^{j-1} e^{-\frac{x}{\eta_{l_i}}}\Big). \tag{A.4}$$

From (A.4), the CDF can be readily obtained as

$$F_S(x) = Q\Big(1+\sum_{k=1}^{K}\sum_{l_1=1}^{K-k+1}\sum_{l_2=l_1+1}^{K-k+2}\cdots\sum_{l_k=l_{k-1}+1}^{K}\Big(\prod_{n=1}^{k}\frac{p_{l_n}}{(1-p_{l_n})}\Big)\sum_{i=1}^{k}\sum_{j=1}^{m_i}\frac{\Omega_{i,j}(-1)^j}{\Gamma(j)}\gamma_l(j,\frac{x}{\eta_{l_i}})\Big). \tag{A.5}$$

Let us assume a set of interfering channel parameters as $\Phi = \{X_G = \{g_i, \forall i\}, X_{\tilde{\alpha}} = \{\tilde{\alpha}_i, \forall i\}\}$, where X_G and $X_{\tilde{\alpha}}$, respectively, denote the set of interfering channels and the set of positions of the interferers. The conditional CDF of S, conditioned on Φ is given by

$$\begin{aligned} Pr\Big(\frac{S}{N+1} < \theta\Big) &= Pr\Big(S < (N+1)\theta\Big) \\ &= E_\Phi\{F_S((N+1)\theta|\Phi)\}. \end{aligned} \tag{A.6}$$

To compute (A.6), we first compute the following expression for $F_S((N+1)\theta|\Phi)$ provided in (A.7) at the top of the next page. In (A.7), we have used series representations for the incomplete gamma function [34, eq. (8.352.6)] and the binomial theorem. To simplify our notation, we define $\widetilde{\sum}[\,\cdot\,] \triangleq \sum_{k=1}^{K}\sum_{l_1}^{K-k+1}\sum_{l_2=l_1+1}^{K-k+2}\cdots\sum_{l_k=l_{k-1}+1}^{K}\big(\prod_{n=1}^{k}\frac{p_{l_n}}{(1-p_{l_n})}\big)[\,\cdot\,]$. Now using the definition of the interferer's total power N, we can have the following expression via the multinomial theorem

$$N^q = (\sum_{i=1}^{M} N_i)^q = \sum_{\substack{j_1,j_2,\cdots,j_M \\ j_1+\cdots+j_M=q}}^{q} \frac{q!}{j_1!j_2!\ldots j_M!}\prod_{t=1}^{M}(N_t)^{j_t}. \tag{A.8}$$

To compute $E_\Phi\{F_S((N+1)\theta)\}$, we use $E_\Phi\{F_S((N+1)\theta)\} = E_{X_{\tilde{\alpha}}}\{\underbrace{E_{X_G}\{F_S((N+1)\theta)|X_{\tilde{\alpha}}\}}_{J_4}\}$, where the inner expression J_4 is computed in (A.9) at the top of the next page. In (A.9), we have assumed that N_t is independent from others. Now having applied the PDF of N_t, which is given by

$$f_{N_t}(x|\alpha_i) = \frac{1}{\Gamma(\tilde{m}_k)(\tilde{\eta}_k)^{\tilde{m}_k}}x^{\tilde{m}_k-1}e^{-\frac{x}{\tilde{\eta}_k}} \tag{A.10}$$

yields

$$J_4 = Q\Big(1+\widetilde{\sum}\sum_{i=1}^{k}\sum_{j=1}^{m_i}\Omega_{i,j}(-1)^j\big(1-e^{-\theta/\eta_{l_i}}\sum_{p=0}^{j-1}(\frac{\theta}{\eta_{l_i}})^p \sum_{q=0}^{p}\sum_{\substack{j_1,j_2,\cdots,j_M \\ j_1+\cdots+j_M=q}}^{q}\frac{1}{(p-q)!}\prod_{t=1}^{M}\frac{1}{j_t!}\frac{\Gamma(j_t+\tilde{m}_t)}{\Gamma(\tilde{m}_t)(\tilde{\eta}_t)^{\tilde{m}_t}} \Big(\frac{\theta}{\eta_{l_i}}+\frac{1}{\tilde{\eta}_t}\Big)^{-(j_t+\tilde{m}_t)}\big)\Big). \tag{A.11}$$

Upon replacing $\tilde{\eta}_t$ with $\tilde{\eta}_t = \frac{P_{I,t}\tilde{n}_t\tilde{d}_{t,R}^{-\epsilon}}{\sigma_n^2}$, (A.11) is evaluated as

$$J_4 = Q\Big(1+\widetilde{\sum}\sum_{i=1}^{k}\sum_{j=1}^{m_i}\Omega_{i,j}(-1)^j\big(1-e^{-\theta/\eta_{l_i}}\sum_{p=0}^{j-1}(\frac{\theta}{\eta_{l_i}})^p \sum_{q=0}^{p}\sum_{\substack{j_1,j_2,\cdots,j_M \\ j_1+\cdots+j_M=q}}^{q}\frac{1}{(p-q)!}\prod_{t=1}^{M}\frac{1}{j_t!}\frac{\Gamma(j_t+\tilde{m}_t)(\tilde{D}_{t,R})^{\tilde{m}_t}}{\Gamma(\tilde{m}_t)(\frac{P_{I,t}\tilde{n}_t}{\sigma_n^2})^{\tilde{m}_t}} \Big(\frac{\theta}{\eta_{l_i}}+\frac{\tilde{D}_{t,R}}{\frac{P_{I,t}\tilde{n}_t}{\sigma_n^2}}\Big)^{-(j_t+\tilde{m}_t)}\big)\Big) \tag{A.12}$$

where $\tilde{D}_{t,R} \triangleq \tilde{d}_{t,R}^{\epsilon}$. The PDF of $\tilde{D}_{t,R}$ derived from the PDF of $\tilde{d}_{t,R}$, which is uniformly distributed within the annulus specified by inner radius, $\chi_r r_{\max}$, and outer radius, $r_{\max}$, is given by

$$f_{\tilde{D}_{t,R}}(x) = \frac{2x^{2/\epsilon-1}}{\epsilon r_{\max}^2[1-\chi_r^2]}, \text{for } \chi_r r_{\max} \le x \le r_{\max}. \tag{A.13}$$

Now using (A.13), we are ready to compute $E_\Phi\{F_S((N+1)\theta)\}$, which is given by

$$E_\Phi\{F_S((N+1)\theta)\} = E_{X_{\tilde{\alpha}}}\{J_4\}. \tag{A.14}$$

Having applied (A.13) into (A.14), we have

$$\begin{aligned} &E_\Phi\{F_S((N+1)\theta)\} = \\ &Q\Big(1+\widetilde{\sum}\sum_{i=1}^{k}\sum_{j=1}^{m_i}\Omega_{i,j}(-1)^j\big(1-e^{-\theta/\eta_{l_i}}\sum_{p=0}^{j-1}(\frac{\theta}{\eta_{l_i}})^p \sum_{q=0}^{p}\sum_{\substack{j_1,j_2,\cdots,j_M \\ j_1+\cdots+j_M=q}}^{q}\frac{1}{(p-q)!}\prod_{t=1}^{M}\frac{1}{j_t!}\frac{\Gamma(j_t+\tilde{m}_t)}{\Gamma(\tilde{m}_t)(\frac{P_{I,t}\tilde{n}_t}{\sigma_n^2})^{\tilde{m}_t}} \underbrace{\int_{\chi_r^\epsilon r_{\max}^\epsilon}^{r_{\max}^\epsilon}(x)^{\tilde{m}_t}\Big(\frac{\theta}{\eta_{l_i}}+\frac{x}{\frac{P_{I,t}\tilde{n}_t}{\sigma_n^2}}\Big)^{-(j_t+\tilde{m}_t)}f_{\tilde{D}_{t,R}}(x)dx}_{J_5}\big)\Big) \end{aligned} \tag{A.15}$$

from which after some manipulations J_5 is computed as follows:

$$\begin{aligned} J_5 = \frac{2\Big(\frac{\theta}{\eta_{l_i}}\Big)^{-(j_t+\tilde{m}_t)}\frac{(r_{\max}^{\epsilon\tilde{m}_t+2})}{\tilde{m}_t+2/\epsilon}}{\epsilon r_{\max}^2[1-\chi_r^2]}\Bigg[&{}_2F_1\Big(\tilde{m}_t+\frac{2}{\epsilon}, j_t+\tilde{m}_t; \tilde{m}_t+\frac{2}{\epsilon}+1; -\frac{r_{\max}^\epsilon\tilde{\eta}_{l_i}\sigma_n^2}{\theta P_{I,t}\tilde{n}_t}\Big) - \\ &(\chi_r^{\epsilon\tilde{m}_t+2}) \\ &{}_2F_1\Big(\tilde{m}_t+\frac{2}{\epsilon}, j_t+\tilde{m}_t; \tilde{m}_t+\frac{2}{\epsilon}+1; -\frac{\chi_r^\epsilon r_{\max}^\epsilon\tilde{\eta}_{l_i}\sigma_n^2}{\theta P_{I,t}\tilde{n}_t}\Big)\Bigg] \end{aligned} \tag{A.16}$$

where we have used [38, eq. (2.2.6.15)]. Replacing J_5 in (A.15) with (A.16), we can have (4).

Appendix B: Derivation of Corollary 3

For the derivation, let us use the distribution provided in (9). That is,

$$\begin{aligned} O_{2,\text{out}}^{\infty}(\theta) \approx Q + Q\sum_{l=1}^{K}\binom{K}{l}(\frac{p}{1-p})^l - \\ \frac{2Q}{\epsilon r_{\max}^2[1-\chi_r^2]}\sum_{l=1}^{K}\binom{K}{l}(\frac{p}{1-p})^l \\ \sum_{m'=0}^{ml-1}\frac{1}{(\tilde{m}M+m')B(\tilde{m}M, m'+1)(\tilde{m}M+2/\epsilon)} \\ (\frac{\mu P}{P_I})^{(\tilde{m}M)}\theta^{-\tilde{m}M}r_{\max}^{\epsilon\tilde{m}M+2}\Bigg[\end{aligned}$$

$$
\begin{aligned}
F_S((N+1)\theta|\Phi) &= Q\Big(1+\widetilde{\sum}\sum_{i=1}^{k}\sum_{j=1}^{m_i}\frac{\Omega_{i,j}(-1)^j}{\Gamma(j)}\gamma(j,(N+1)\theta/\eta_{l_i})\Big)\\
&= Q\Big(1+\widetilde{\sum}\sum_{i=1}^{k}\sum_{j=1}^{m_i}\frac{\Omega_{i,j}(-1)^j}{\Gamma(j)}\Gamma(j)\big(1-e^{-(N+1)\theta/\eta_{l_i}}\sum_{p=0}^{j-1}\frac{1}{p!}\big(\frac{(N+1)\theta}{\eta_{l_i}}\big)^p\big)\Big)\\
&= Q\Big(1+\widetilde{\sum}\sum_{i=1}^{k}\sum_{j=1}^{m_i}\Omega_{i,j}(-1)^j\big(1-e^{-(N+1)\theta/\eta_{l_i}}\sum_{p=0}^{j-1}\frac{1}{p!}\big(\frac{\theta}{\eta_{l_i}}\big)^p(N+1)^p\big)\Big)\\
&= Q\Big(1+\widetilde{\sum}\sum_{i=1}^{k}\sum_{j=1}^{m_i}\Omega_{i,j}(-1)^j\big(1-e^{-(N+1)\theta/\eta_{l_i}}\sum_{p=0}^{j-1}\frac{1}{p!}\big(\frac{\theta}{\eta_{l_i}}\big)^p\sum_{q=0}^{p}\binom{p}{q}(N)^q\big)\Big). \qquad \text{(A.7)}
\end{aligned}
$$

$$
\begin{aligned}
J_4 &= Q\Big(1+\widetilde{\sum}\sum_{i=1}^{k}\sum_{j=1}^{m_i}\Omega_{i,j}(-1)^j\\
&\quad\big(1-e^{-\theta/\eta_{l_i}}\sum_{p=0}^{j-1}\frac{1}{p!}\big(\frac{\theta}{\eta_{l_i}}\big)^p\sum_{q=0}^{p}\binom{p}{q}\sum_{\substack{j_1,j_2,\cdots,j_M\\ j_1+\cdots+j_M=q}}^{q}\frac{q!}{j_1!j_2!\ldots j_M!}\prod_{t=1}^{M}\int_0^\infty e^{-\theta x/\eta_{l_i}}(x)^{j_t}f_{N_t}(x|\alpha_i)dx\big)\Big)\\
&= Q\Big(1+\widetilde{\sum}\sum_{i=1}^{k}\sum_{j=1}^{m_i}\Omega_{i,j}(-1)^j\\
&\quad\big(1-e^{-\theta/\eta_{l_i}}\sum_{p=0}^{j-1}\big(\frac{\theta}{\eta_{l_i}}\big)^p\sum_{q=0}^{p}\sum_{\substack{j_1,j_2,\cdots,j_M\\ j_1+\cdots+j_M=q}}^{q}\frac{1}{(p-q)!}\prod_{t=1}^{M}\frac{1}{j_t!}\int_0^\infty e^{-\theta x/\eta_{l_i}}(x)^{j_t}f_{N_t}(x|\alpha_i)dx\big)\Big). \qquad \text{(A.9)}
\end{aligned}
$$

$$
\begin{aligned}
&{}_2F_1\big(\tilde{m}M+\frac{2}{\epsilon},\tilde{m}M+m';\tilde{m}M+\frac{2}{\epsilon}+1;-\frac{r_{\max}^{\epsilon}\mu P}{\theta P_I}\big)-\\
&\quad\chi_r^{\epsilon\tilde{m}M+2}\\
&{}_2F_1\big(\tilde{m}M+\frac{2}{\epsilon},\tilde{m}M+m';\tilde{m}M+\frac{2}{\epsilon}+1;-\frac{\chi_r^{\epsilon}r_{\max}^{\epsilon}\mu P}{\theta P_I}\big)\Big]. \qquad \text{(B.1)}
\end{aligned}
$$

Since as $P\to\infty$, we have $|z|>1$ in the representation of ${}_2F_1(a,b;c;-z)$ in our problem, with the constraint $a-b\notin\mathbb{Z}$, we use the following equivalent form for ${}_2F_1(a,b;c;-z)$ [39, eq. (7.2.1.6)]:

$$
\begin{aligned}
&{}_2F_1(a,b;c;-z)=\\
&\frac{\Gamma(b-a)\Gamma(c)z^{-a}}{\Gamma(b)\Gamma(c-a)}{}_2F_1(a,1+a-c;1+a-b;1/z)+\\
&\frac{\Gamma(a-b)\Gamma(c)z^{-b}}{\Gamma(a)\Gamma(c-a)}{}_2F_1(b,1+b-c;1+b-a;1/z) \qquad \text{(B.2)}
\end{aligned}
$$

where ${}_2F_1(a,b;c;-z)=\sum_{k=0}^{\infty}\frac{(a)_k(b)_k}{\Gamma(k+1)(c)_k}(-z)^k$ [39, eq. (7.2.1.1)] with $(a)_k$ denoting the Pochhammer symbol defined by $(a)_k\stackrel{\triangle}{=}a(a-1)\cdots(a-k+1)$. Now applying the corresponding variables, we can approximate (B.2) as:

$$
{}_2F_1(a,b;c;-z)\approx\frac{\Gamma(b-a)\Gamma(c)z^{-a}}{\Gamma(b)\Gamma(c-a)}+\frac{\Gamma(a-b)\Gamma(c)z^{-b}}{\Gamma(a)\Gamma(c-b)} \qquad \text{(B.3)}
$$

since ${}_2F_1(a,1+a-c;1+a-b;1/z)=\sum_{k=0}^{\infty}\frac{(a)_k(1+a-c)_k}{\Gamma(k+1)(1+a-b)_k}(z)^{-k}\approx 1$ and ${}_2F_1(b,1+b-c;1+b-a;1/z)=\sum_{k=0}^{\infty}\frac{(b)_k(1+b-c)_k}{\Gamma(k+1)(1+b-a)_k}(z)^{-k}\approx 1$ as $|z|\gg 1$. We can further approximate (B.3) as:

$$
\begin{aligned}
{}_2F_1(a,b;c;-z)&\approx\frac{\Gamma(b-a)\Gamma(c)z^{-a}}{\Gamma(b)\Gamma(c-a)}+\frac{\Gamma(a-b)\Gamma(c)z^{-b}}{\Gamma(a)\Gamma(c-b)}\\
&\approx\frac{\Gamma(a-b)\Gamma(c)z^{-b}}{\Gamma(a)\Gamma(c-b)} \qquad \text{(B.4)}
\end{aligned}
$$

for $|z|\gg 1$ and $a>b$. Using (B.4), we can have

$$
\begin{aligned}
&\sum_{m'=0}^{ml-1}\frac{\theta^{-\tilde{m}M}(r_{\max})^{\epsilon b_1}{}_2F_1\big(b_1,b_2;b_1+1;-\frac{r_{\max}^{\epsilon}\mu}{\theta P_I}\big)}{b_1B(\tilde{m}M,m'+1)b_2}\big(\frac{\mu P}{P_I}\big)^{(\tilde{m}M)}\\
&\approx\frac{\Gamma(\frac{2}{\epsilon})\Gamma(b_1+1)}{(\tilde{m}M)B(\tilde{m}M,m'+1)(b_1)\Gamma(b_1)\Gamma(\frac{2}{\epsilon}+1)}\Big(\frac{r_{\max}^{\epsilon}\mu P}{\theta P_I}\Big)^{-\tilde{m}M}\\
&\theta^{-\tilde{m}M}(r_{\max})^{\epsilon b_1}\big(\frac{\mu P}{P_I}\big)^{(\tilde{m}M)} \qquad \text{(B.5)}
\end{aligned}
$$

where $b_1\stackrel{\triangle}{=}\tilde{m}M+\frac{2}{\epsilon}$, $b_2\stackrel{\triangle}{=}\tilde{m}M+m'$. After some manipulations, (B.5) is evaluated as follows:

$$
\begin{aligned}
&\sum_{m'=0}^{ml-1}\frac{\theta^{-\tilde{m}M}(r_{\max})^{\epsilon b_1}{}_2F_1\big(b_1,b_2;b_1+1;-\frac{r_{\max}^{\epsilon}\mu}{\theta P_I}\big)}{b_1B(\tilde{m}M,m'+1)b_2}\big(\frac{\mu}{P_I}\big)^{(\tilde{m}M)}\\
&\approx\frac{\epsilon r_{\max}^2}{2}. \qquad \text{(B.6)}
\end{aligned}
$$

Similarly, we can have

$$
\sum_{m'=0}^{ml-1}\frac{\theta^{-\tilde{m}M}\chi_r^{\epsilon b_1}r_{\max}^{\epsilon b_1}{}_2F_1\big(b_1,b_2;b_1+1;-\frac{\chi_r^{\epsilon}r_{\max}^{\epsilon}\mu}{\theta P_I}\big)}{(\tilde{m}M+m')B(\tilde{m}M,m'+1)(\tilde{m}M+2/\epsilon)}\big(\frac{\mu P}{P_I}\big)^{(\tilde{m}M)}
$$

$$\approx \frac{\epsilon \chi_r^2 r_{\max}^2}{2}. \quad \text{(B.7)}$$

Collecting Eqs. (B.6) and (B.7), we can verify that $Q_{2,\text{out}}^{\infty}(\theta) \approx Q$ as $P \to \infty$.

Appendix C: Derivation of (12)

To compute the ABER, we first derive $F_\lambda(x)$ from $O_{\text{out}}(x)$ as in (C.1) at the top of the next page. In (C.1), $c_1 \triangleq \frac{P_l}{r_{\max}^{\epsilon} \mu P}$ and $c_2 \triangleq \frac{P_l}{\chi_r^{\epsilon} r_{\max}^{\epsilon} \mu P}$. Now substituting (C.1) into (11), we have (C.2) at the top of the next page. In (C.2), $c_3 \triangleq \tilde{m}M + n - m' + 1/2$. To compute K_1, we use the following equivalent expression using the MeijerG function

$$x^{-c_3} {}_2F_1\Big(\tilde{m}M + \frac{2}{\epsilon}, \tilde{m}M + n; \tilde{m}M + \frac{2}{\epsilon} + 1; -\frac{1}{c_1 x}\Big) = \frac{(c_1)^{c_3}(\tilde{m}M + 2/\epsilon)}{\Gamma(\tilde{m}M + n)} G_{2,2}^{2,1}\Big(\begin{matrix} 1 - c_3, & \tilde{m}M + 2/\epsilon + 1 - c_3 \\ \tilde{m}M + 2/\epsilon - c_3, & \tilde{m}M + n - c_3 \end{matrix} \Big| c_1 x \Big). \quad \text{(C.3)}$$

We also use the following equivalent form for

$$e^{-x(1+\frac{1}{\eta})} = G_{0,1}^{1,0}\Big(\begin{matrix} \cdot \\ 0 \end{matrix} \Big| (1 + \frac{1}{\eta})x \Big). \quad \text{(C.4)}$$

Then, we can have for K_1 as

$$K_1 = \frac{(1+\frac{1}{\eta})^{-1} c_1^{c_3} (\tilde{m}M + 2/\epsilon)}{\Gamma(\tilde{m}M + n)} G_{3,2}^{2,2}\Big(\begin{matrix} 1 - c_3, 0, \tilde{m}M + 2/\epsilon + 1 - c_3 \\ \tilde{m}M + 2/\epsilon - c_3, \tilde{m}M + n - c_3 \end{matrix} \Big| \frac{c_1}{(1+\frac{1}{\eta})} \Big) \quad \text{(C.5)}$$

where we have used [39, eq. (2.241.2)]. Similarly, K_2 can be obtained as

$$K_2 = \frac{(1+\frac{1}{\eta})^{-1} c_2^{c_3} (\tilde{m}M + 2/\epsilon)}{\Gamma(\tilde{m}M + n)} G_{3,2}^{2,2}\Big(\begin{matrix} 1 - c_3, 0, \tilde{m}M + 2/\epsilon + 1 - c_3 \\ \tilde{m}M + 2/\epsilon - c_3, \tilde{m}M + n - c_3 \end{matrix} \Big| \frac{c_2}{(1+\frac{1}{\eta})} \Big). \quad \text{(C.6)}$$

Having applied (C.5) and (C.6) into (C.2) and some manipulations, we can readily obtain (12).

Appendix D: Derivation of Theorem 2

We first compute $\tilde{F}_\lambda(x) \triangleq 1 - F_\lambda(x)$ from (C.1), which is given by (D.1) at the bottom of the next page. Note that in the derivation of (D.1), we used the similar derivations employed in the derivation of the ABER. After using again [39, eq. (2.241.2)], Jensen's inequality, and several properties of the MeijerG function, we can readily derive (16).

Appendix E: Derivation of (16)

We use an approximated distribution (E.1) at the bottom of the next page for the SINR, which can be extracted from (9). We then use the definition of the ASE as follows:

$$R_1^{\infty} = \frac{1}{\log(2)} \int_0^{\infty} \frac{\tilde{F}_{1,\lambda}^{\infty}(x)}{1+x} dx. \quad \text{(E.2)}$$

To compute (E.2), we also convert the following function in terms of the MeijerG function

$$\frac{x^{-\tilde{m}M}}{1+x} = G_{1,1}^{1,1}\Big(\begin{matrix} -\tilde{m}M \\ -\tilde{m}M \end{matrix} \Big| x \Big) \quad \text{(E.3)}$$

and again use (C.3). After applying again [39, eq. (2.241.2)] and some manipulations, (19) can be derived.

References

[1] S. Arad and J. Hoadley, "Systems and methods optimizing backhaul transport," Patent Application Publication US 2014/0 160 939 A1, Jun. 12, 2014.

[2] S. Chia, M. Gasparroni, and P. Brick, "The next challenge for cellular networks: Backhaul," *IEEE Microw. Mag.*, vol. 10, no. 5, pp. 54–66, 2009.

[3] S. Hur, T. Kim, D. J. Love, J. V. Krogmeier, T. A. Thomas, and A. Ghosh, "Millimeter wave beamforming for wireless backhaul and access in small cell networks," *IEEE Trans. Commun.*, vol. 61, pp. 4391–4403, Oct. 2013.

[4] M. Coldrey, H. Koorapaty, J. Berg, Z. Ghebretensae, J. Hansryd, A. Derneryd, and S. Falahati, "Small-cell wireless backhauling: A non-line-of-sight approach for point-to-point microwave links," in *Proc. IEEE Veh. Tech. Conf.*, Quebec City, Canada, Sep. 2012, pp. 1–5.

[5] O. Tipmongkolsilp, S. Zaghloul, and A. Jukan, "The evolution of cellular backhaul technologies: Current issues and future trends," *IEEE Commun. Surveys Tutorials*, vol. 13, no. 1, pp. 97–113, 1st Quart., 2011.

[6] P. Ishwar, R. Puri, K. Ramchandran, and S. S. Pradhan, "On rate-constrained distributed estimation in unreliable sensor networks," *IEEE J. Sel. Areas Commun.*, vol. 23, no. 4, pp. 765–775, Apr. 2005.

[7] O. Simeone, O. Somekh, E. Erkip, H. V. Poor, and S. Shamai, "Robust communication via decentralized processing with unreliable backhaul links," *IEEE Trans. Inf. Theory*, vol. 57, pp. 4187–4201, Jul. 2011.

[8] Y. Li, X. Wang, S. Zhou, and S. Alshomrani, "Uplink coordinated multi-point reception with limited backhaul via cooperative group decoding," *IEEE Trans. Wireless Commun.*, vol. 13, no. 6, pp. 3017–3030, Jun. 2014.

[9] J. Du, M. Xiao, M. Skoglund, and M. Medard, "Wireless multicast relay networks with limited-rate source-conferencing," *IEEE J. Sel. Areas Commun.*, vol. 31, no. 8, pp. 1390–1401, Aug. 2013.

[10] J. Du, M. Xiao, and M. Skoglund, "Cooperative network coding strategies for wireless relay networks with backhaul," *IEEE Trans. Commun.*, vol. 60, pp. 2502–2514, Sep. 2011.

[11] A. D. Coso and S. Simoens, "Distributed compression for mimo coordinated networks with a backhaul constraint," *IEEE Trans. Wireless Commun.*, vol. 8, no. 9, pp. 4698–4709, Sep. 2011.

[12] O. Simeone, O. Somekh, H. Poor, and S. Shamai, "Enhancing uplink throughput via local base station cooperation," in *Proc. Asilomar Conf. Signals, Syst., Comput.*, Pacific Grove, CA, Nov. 2008, pp. 116–120.

[13] E. Aktas, J. Evans, and S. Hanley, "Distributed decoding in a cellular multiple-access channel," *IEEE Trans. Wireless Commun.*, vol. 7, no. 1, pp. 241–250, Jun. 2008.

[14] Z. Mayer, J. Li, A. Papadogiannis, and T. Svensson, "On the impact of backhaul channel reliability on cooperative wireless networks," in *Proc. IEEE Int. Conf. Commun.*, Budapest, Hungary, Jun. 2013, pp. 5284–5289.

[15] J. Guo, S. Durrani, and X. Zhou, "Performance analysis of arbitrarily-shaped underlay cognitive networks: Effects of secondary user activity protocols," *IEEE Trans. Commun.*, vol. 63, pp. 376–389, Feb. 2015.

[16] C.-H. Lee and M. Haenggi, "Interference and outage in Poisson cognitive networks," *IEEE Trans. Wireless Commun.*, vol. 11, no. 4, pp. 1392–1401, Apr. 2012.

[17] F. Paisana, N. Marchetti, and L. DaSilva, "Radar, TV and cellular bands: Which spectrum access techniques for which bands?" *IEEE Commun. Surveys Tuts.*, vol. 16, no. 3, pp. 1193–1220, 2014.

[18] A. Hasan and J. G. Andrews, "The guard zone in wireless ad hoc networks," *IEEE Trans. Wireless Commun.*, vol. 6, pp. 897–906, Mar. 2007.

[19] D. Torrieri and M. C. Valenti, "The outage probability of a finite Ad Hoc network in Nakagami fading," *IEEE Trans. Commun.*, vol. 60, pp. 2960–2970, Dec. 2012.

[20] J. Guo, S. Durrani, and X. Zhou, "Outage probability in arbitrarily-shaped finite wireless networks," *IEEE Trans. Commun.*, vol. 62, pp. 699–712, Feb. 2014.

$$F_{\lambda}(x) = Q + Q\sum_{l=1}^{K}\binom{K}{l}(\frac{p}{1-p})^{l} - \frac{2Q}{\epsilon r_{\max}^{2}[1-\chi_r^2]}\sum_{l=1}^{K}\binom{K}{l}(\frac{p}{1-p})^{l}$$
$$\sum_{m'=0}^{ml-1}(\frac{1}{\eta})^{m'}\sum_{n=0}^{m'}\binom{m'}{n}\frac{\Gamma(\tilde{m}M+n)(\tilde{\eta})^{n}\left(\frac{P_I}{\mu P}\right)^{-(\tilde{m}M+n)}e^{-\frac{x}{\eta}}(x)^{-(\tilde{m}M+n-m')}r_{\max}^{\epsilon\tilde{m}M+2}}{\Gamma(\tilde{m}M)\Gamma(m'+1)(\tilde{m}M+2/\epsilon)}$$
$$\Bigg[{}_2F_1\big(\tilde{m}M+\frac{2}{\epsilon},\tilde{m}M+n;\tilde{m}M+\frac{2}{\epsilon}+1;-\frac{1}{c_1x}\big)-$$
$$\chi_r^{\epsilon\tilde{m}M+2}\,{}_2F_1\big(\tilde{m}M+\frac{2}{\epsilon},\tilde{m}M+n;\tilde{m}M+\frac{2}{\epsilon}+1;-\frac{1}{c_2x}\big)\Bigg]. \tag{C.1}$$

$$S_b = \frac{Q}{2} + \frac{Q}{2}\sum_{l=1}^{K}\binom{K}{l}(\frac{p}{1-p})^{l} - \frac{Q}{\sqrt{\pi}\epsilon r_{\max}^{2}[1-\chi_r^2]}\sum_{l=1}^{K}\binom{K}{l}(\frac{p}{1-p})^{l}$$
$$\sum_{m'=0}^{ml-1}(\frac{1}{\eta})^{m'}\sum_{n=0}^{m'}\binom{m'}{n}\frac{\Gamma(\tilde{m}M+n)(\tilde{\eta})^{n}\left(\frac{P_I}{\mu P}\right)^{-(\tilde{m}M+n)}(r_{\max})^{\epsilon\tilde{m}M+2}}{\Gamma(\tilde{m}M)\Gamma(m'+1)(\tilde{m}M+2/\epsilon)}$$
$$\Bigg[\underbrace{\int_0^{\infty}e^{-x(1+\frac{1}{\eta})}x^{-c_3}\,{}_2F_1\big(\tilde{m}M+\frac{2}{\epsilon},\tilde{m}M+n;\tilde{m}M+\frac{2}{\epsilon}+1;-\frac{1}{c_1x}\big)dx}_{K_1}-$$
$$\chi_r^{\epsilon\tilde{m}M+2}\underbrace{\int_0^{\infty}e^{-x(1+\frac{1}{\eta})}x^{-c_3}\,{}_2F_1\big(\tilde{m}M+\frac{2}{\epsilon},\tilde{m}M+n;\tilde{m}M+\frac{2}{\epsilon}+1;-\frac{1}{c_2x}\big)\Bigg]dx}_{K_2}. \tag{C.2}$$

$$\tilde{F}_{\lambda}(x) = \frac{2Q}{\epsilon r_{\max}^{2}[1-\chi_r^2]}\sum_{l=1}^{K}\binom{K}{l}(\frac{p}{1-p})^{l}$$
$$\sum_{m'=0}^{ml-1}(\frac{1}{\eta})^{m'}\sum_{n=0}^{m'}\binom{m'}{n}\frac{\Gamma(\tilde{m}M+n)(\tilde{\eta})^{n}\left(\frac{P_I}{\mu P}\right)^{-(\tilde{m}M+n)}e^{-\frac{x}{\eta}}(x)^{-(\tilde{m}M+n-m')}(r_{\max})^{\epsilon\tilde{m}M+2}}{\Gamma(\tilde{m}M)\Gamma(m'+1)(\tilde{m}M+2/\epsilon)}$$
$$\Bigg[{}_2F_1\big(\tilde{m}M+\frac{2}{\epsilon},\tilde{m}M+n;\tilde{m}M+\frac{2}{\epsilon}+1;-\frac{1}{c_1x}\big)-$$
$$\chi_r^{\epsilon\tilde{m}M+2}\,{}_2F_1\big(\tilde{m}M+\frac{2}{\epsilon},\tilde{m}M+n;\tilde{m}M+\frac{2}{\epsilon}+1;-\frac{1}{c_2x}\big)\Bigg]. \tag{D.1}$$

$$F_{1,\lambda}^{\infty}(x) = 1 - \frac{2Q}{\epsilon r_{\max}^{2}[1-\chi_r^2]}\sum_{l=1}^{K}\binom{K}{l}(\frac{p}{1-p})^{l}$$
$$\sum_{m'=0}^{ml-1}\frac{(r_{\max})^{\epsilon\tilde{m}M+2}}{(\tilde{m}M+m')B(\tilde{m}M,m'+1)(\tilde{m}M+2/\epsilon)}\big(\kappa\mu\big)^{(\tilde{m}M)}x^{-\tilde{m}M}$$
$$\Bigg[{}_2F_1\big(\tilde{m}M+\frac{2}{\epsilon},\tilde{m}M+m';\tilde{m}M+\frac{2}{\epsilon}+1;-\frac{r_{\max}^{\epsilon}\kappa\mu}{x}\big)-$$
$$\chi_r^{\epsilon\tilde{m}M+2}\,{}_2F_1\big(\tilde{m}M+\frac{2}{\epsilon},\tilde{m}M+m';\tilde{m}M+\frac{2}{\epsilon}+1;-\frac{\chi_r^{\epsilon}r_{\max}^{\epsilon}\kappa\mu}{x}\big)\Bigg] = 1-\tilde{F}_{1,\lambda}^{\infty}(x). \tag{E.1}$$

[21] K. J. Kim, T. Q. Duong, M. Elkashlan, P. L. Yeoh, H. V. Poor, and M. H. Lee, "Spectrum sharing single-carrier in the presence of multiple licensed receivers," *IEEE Trans. Wireless Commun.*, vol. 12, no. 10, pp. 5223–5235, Oct. 2013.

[22] Z. Mayer, J. Li, A. Papadogiannis, and T. Svensson, "On the impact of control channel reliability on coordinated multi-point transmission," *EURASIP Journal on Wireless Communications and Networking*, no. 2014:28, 2014.

[23] F. Pantisano, M. Bennis, W. Saad, M. Debbah, and M. Latva-aho, "On the impact of heterogeneous backhauls on coordinated multipoint transmission in femtocell networks," in *Proc. IEEE Int. Conf. Commun.*, Ottawa, Canada, June 2012, pp. 5064–5096.

[24] F. H. Panahi and T. Ohtsuki, "Analytical modeling of cognitive heterogeneous cellular networks over Nakagami-m fading," *EURASIP Journal on Wireless Communications and Networking*, no. 2015:16, 2015.

[25] A. Lozano, A. M. Tulino, and S. Verdú, "High-SNR power offset in multiantenna communication," in *Proc. IEEE Int. Symp. Inf. Theory*, Chicago, USA, Jun. 2004, p. 287.

[26] P. Misra, B. P. Burke, and M. M. Pratt, "GPS performance in navigation," *Proc. IEEE*, vol. 87, no. 1, pp. 65–85, Jan. 1999.

[27] M. P. Wylie and J. Holtzman, "The non-line of sight problem in mobile location estimation," in *Proc. IEEE Int. Conf. Univer. Pers. Commun.*, Cambridge, MA, Sep. 1996, pp. 827 – 831.

[28] C. Ma, R. Klukas, and G. Lachapelle, "A nonline-of-sight error-mitigation method for TOA measurements," *IEEE Trans. Veh. Technol.*, vol. 56, no. 2, pp. 641–651, Mar. 2007.

[29] R. Tanbourgi, S. Singh, J. G. Andrew, and F. K. Jondral, "A tractable model for non-coherent joint-transmission base station cooperation," *IEEE Trans. Wireless Commun.*, vol. 13, no. 9, pp. 4959 –4973, Sep. 2014.

[30] T. A. Tsiftsis, G. K. Karagiannidis, N. C. Sagias, and S. A. Kotsopoulos, "Performance of MRC diversity receivers over correlated nakagami-m fading channels," in *Proc. Communication Systems, Networks and Digital Signal Processing*, Patras, Greece, Jul. 2006.

[31] A. Maaref and R. Annavajjala, "The gamma variate with random shape parameter and some applications," *IEEE Commun. Lett.*, vol. 12, pp. 1146–1148, Dec. 2011.

[32] J. M. Romero-Jerez and A. J. Goldsmith, "Receive antenna array stretegies in fading and interference: An outage probability comparison," *IEEE Trans. Wireless Commun.*, vol. 7, no. 3, pp. 920–932, Mar. 2008.

[33] H. Yu, I.-H. Lee, and G. L. Stuber, "Outage probability of decode-and-forward cooperative relaying systems with co-channel interference," *IEEE Trans. Wireless Commun.*, vol. 11, no. 1, pp. 266–274, Jan. 2011.

[34] I. S. Gradshteyn and I. M. Ryzhik, *Table of Integrals, Series, and Products*. New York: Academic Press, 2007.

[35] N. C. Sagias, G. S. Tombras, and G. K. Karagiannidis, "New results for the Shannon channel capacity in generalized fading channels," *IEEE Commun. Lett.*, vol. 9, no. 2, pp. 97 –99, Feb. 2005.

[36] H. A. Suraweera, P. J. Smith, and M. Shafi, "Capacity limits and performance analysis of cognitive radio with imperfect channel knowledge," *IEEE Trans. Veh. Technol.*, vol. 59, no. 4, pp. 1811–1822, May 2010.

[37] A. Erdelyi, *Higher Transcendental Functions*. New York, N.Y.: McGraw-Hill Book Company, 1953.

[38] A. P. Prudnikov, Y. A. Brychkov, and O. I. Marichev, *Integral and Series. Vol. 1: Elementary Functions*, 4th ed. London: Gordon and Breach, 1998.

[39] ——, *Integrals and Series. Vol. 3: More Special Functions*, 3rd ed. New York: Gordon and Breach Science, 1990.

Kyeong Jin Kim (SM'11) received the M.S. degree from the Korea Advanced Institute of Science and Technology (KAIST) in 1991 and the M.S. and Ph.D. degrees in electrical and computer engineering from the University of California, Santa Barbara in 2000. During 1991-1995, he was a research engineer at the video research center of Daewoo Electronics, Ltd., Korea. In 1997, he joined the data transmission and networking laboratory, University of California, Santa Barbara. After receiving his degrees, he joined the Nokia research center (NRC) and Nokia Inc., Dallas, TX, as a senior research engineer, where he was, from 2005 to 2009, an L1 specialist. During 2010-2011, he was an Invited Professor at Inha University, Korea. Since 2012, he works as a senior principal research staff in the Mitsubishi Electric Research Laboratories (MERL), Cambridge, MA. His research has been focused on the transceiver design, resource management, scheduling in the cooperative wireless communications systems, cooperative spectrum sharing system, physical layer secrecy system, and device-to-device communications.

Dr. Kim currently serves as an editor for the IEEE COMMUNICATIONS LETTERS and INTERNATIONAL JOURNAL OF ANTENNAS AND PROPAGATION. He also served as guest editors for the EURASIP JOURNAL ON WIRELESS COMMUNICATIONS AND NETWORKING: Special Issue on "Cooperative Cognitive Networks" and IET COMMUNICATIONS: Special Issue on "Secure Physical Layer Communications". He serves a TPC chair for the IEEE GLOBECOM 2013, 2014, and 2015 Workshop on Trusted Communications with Physical Layer Security.

Philip V. Orlik (SM'97) was born in New York, NY in 1972. He received the B.E. degree in 1994 and the M.S. degree in 1997 both from the State University of New York at Stony Brook. In 1999 he earned his Ph. D. in electrical engineering also from SUNY Stony Brook.

In 2000 he joined Mitsubishi Electric Research Laboratories Inc. located in Cambridge, MA where he is currently the Team Leader of the Mobile Systems Group. His primary research focus is on advanced wireless and mobile communications, sensor networks, ad hoc networking and UWB. Other research interests include vehicular/car-to-car communications, mobility modeling, performance analysis, and queuing theory.

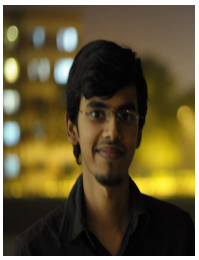

Talha Ahmed Khan (S'xx) graduated with a B.Sc. in electrical engineering from University of Engineering and Technology Lahore, Pakistan. He received the M.S.E. degree in electrical and computer engineering from The University of Texas at Austin, where he is currently working towards his Ph.D. degree. His research interests include wireless communications, stochastic geometry applications, millimeter wave communications, and energy harvesting. He has held internship positions at Broadcom in 2013, and at Mitsubishi Electric Research Labs in 2014.